Sulfonate-based single-ion conducting polymer electrolytes for lithium metal batteries

By

Aaron Robertson

A thesis submitted to the University of Ottawa

in conformity with the requirements for the degree of Master of Applied Science

Department of Chemical and Biological Engineering, Faculty of Engineering, University of Ottawa

Supervised by: Dr. Kelly Meek

uOttawa

ABSTRACT

Solid-state batteries can offer improved energy density and safety relative to conventional liquid lithium-ion batteries. In particular, single-ion polymer electrolytes (SIPEs) offer high ionic conductivity, effectively suppressing lithium dendrite growth. In this study, a series of SIPEs composed of poly(ethylene oxide) methyl ether methacrylate (PEGMA) and poly(lithium 4-styrene sulfonate) (PLSS) were synthesized. These random copolymers (RCPs) were prepared via reversible addition−fragmentation chain transfer (RAFT) polymerization at six different compositions with PLSS content ranging from 12 to 75 mol%.

First, the chemical and thermal properties of the RCPs were fully characterized; all RCPs were found to have sufficiently high thermal degradation temperatures, with glass transition temperatures below room temperature. Next, PEGMA-*r*-PLSS films were prepared and tested for ionic conductivity using electrochemical impedance spectroscopy (EIS); copolymers exhibited high conductivity of 2.2 x 10^{-5} S cm^{-1} at room temperature, reaching a maximum of 2.3 x 10^{-4} S cm^{-1} at 70 °C. As PEGMA is the flexible, ion-transporting polymer, while PLSS contributes lithium ions and rigidity from functionalized polystyrene, the RCP with the lowest PLSS content (i.e., PEGMA-*r*-PLSS-12) exhibited the highest ionic conductivity but did not form free-standing films. Alternatively, films with more moderate amounts of PLSS resulted in both sufficient mechanical and ion transport properties. PEGMA-*r*-PLSS-50, which has the reported optimal ethylene oxide to lithium-ion ratio (EO:Li^+) of 9:1, achieved the second highest room temperature conductivity (1.6 x 10^{-6} S cm^{-1}) and second highest ion conductivity at 70 °C (1.4 x 10^{-4} S cm^{-1}), while also forming free-standing SIPEs.

Considering the need to balance conductivity with mechanical properties, two methods were explored to improve the RCP SIPEs: (1) blending RCPs with poly(lithium vinyl sulfonate) (PLVS) and (2) synthesizing block copolymer analogs of the RCP (PEGMA-*b*-PLSS). Despite the low glass transition temperature of PLVS, it was not found to improve ion conductivity of PEGMA-*r*-PLSS-12. Due to differences in polymer solubility, polymer miscibility may be an issue at higher PEGMA compositions. Block copolymer synthesis is ongoing. PEGMA-*r*-PLSS copolymers show strong potential as a candidate for SIPEs for lithium metal batteries when synthesized with an optimal 9:1 ratio of EO:Li^+ and conductivity may be further improved by transitioning to a block structure.

Statement of Contributions of Collaborators

I hereby declare that I am the sole author of this thesis.

The entire thesis was written by me with editorial corrections from Dr. Kelly Meek.

Polymer synthesis, ion exchange, and characterization (nuclear magnetic resonance spectroscopy, Fourier transform infrared spectroscopy, and thermogravimetric analysis) were done by me.

Dr. Hilal Al-Salih conducted ionic conductivity measurements (Ch. 3 and 4) and differential scanning calorimetry (Ch. 4) at the National Research Council under the supervision of Dr. Yaser Abu-Lebdeh. Data analysis and figure preparation were done by me.

Kerri Warbanski, MASc, at Concordia University conducted differential scanning calorimetry and gel permeation chromatography (Ch. 3). Data analysis and figure preparation were done by me.

Dr. Menandro Cruz conducted gel permeation chromatography (Ch. 5) under supervision of Dr. Benoit Lessard at the University of Ottawa. Data analysis and figure preparation were done by me.

Acknowledgements

I first would like to express my deepest gratitude to my supervisor, Dr. Kelly Meek, for her exceptional guidance, encouragement, and support throughout the course of my master's thesis. Her expertise, insightful feedback, and patience were invaluable in helping me navigate challenges and refine my work. Dr. Meek's dedication to fostering my academic growth and her enthusiasm for research have been truly inspiring, and I feel incredibly fortunate to have had the opportunity to work under her mentorship.

I would also like to thank Dr. George Psofogiannakis and Dr. Andrew Anstey for being my master's defense committee. Reviewing is lengthy process, and I truly appreciate their time, effort, and thoughtful feedback. I would also like to thank my fellow lab mates: Asma, Alannah, Maryam and Parisa. I would like to extend my thanks to Alannah for her support in the lab and her assistance with running samples at Concordia University. I am also deeply grateful to Asma for her thoughtful advice and guidance on my projects in the lab.

I want to acknowledge Dr. Hilal Al-Salih at the National Research Council for conducting the ionic conductivity measurements with permission from Dr. Yaser Abu-Lebdeh. These measurements are time-consuming and require significant expertise, and I am deeply grateful for Dr. Al-Salih's skill and dedication. I also thank Dr. Al-Salih for performing the differential scanning calorimetry measurements featured in Chapter 4. Also, thank you to Dr. Menandro Cruz at the University of Ottawa for conducting the gel permeation chromatography measurements presented in Chapter 5.

Nomenclature

AIBN	2,2′-azobis-(isobutyronitrile)
APS	Ammonium persulfate
ATRP	Atom transfer radical polymerization
$CDCl_3$	Deuterated Chloroform
CTA	Chain transfer agent
DIPE	Dual-ion polymer electrolytes
DIW	Deionized water
DMF	Dimethylformamide
DMSO	Dimethyl sulfoxide
DSC	Differential scanning calorimetry
EIS	Electrochemical impedance spectroscopy
EO:Li+	Ethylene oxide repeat units to lithium-ion ratio
ESW	Electrochemical stability window
EV	Electric vehicle
FTIR	Fourier transform infrared spectroscopy
GPC	Gel Permeation Chromatography
LIB	Lithium-ion battery
LiBr	Lithium bromide
LiOH	Lithium hydroxide
$LiPF_6$	Lithium hexafluorophosphate
LiTFSI	Lithium bis(trifluoromethanesulfonyl)imide
LMB	Lithium metal battery
MEHQ	Mequinol
MW	Molecular weight
NaSS	Sodium styrene sulfonate
NMR	Nuclear Magnetic Resonance spectroscopy
PDI	Polydispersity Index
PEGMA	Poly(ethylene oxide) methyl ether methacrylate
PEO	Polyethylene oxide

PLSS	Poly(lithium 4-styrenesulfonate)
PLVS	Poly(lithium vinyl sulfonate)
PS	Polystyrene
PSS	Polystyrene sulfonate
PVSA	Polyvinyl sulfonic acid
RAFT	Reversible addition-fragmentation chain transfer polymerization
RCP	Random copolymer
SIPEs	SIPEs
SPE	Solid polymer electrolyte
T_d	Degradation temperature
TFSI	(trifluoromethanesulfonyl)imide
T_g	Glass transition temperature
T_g/T	Reduced temperature
TGA	Thermogravimetric analysis
VSA	Vinyl sulfonic acid

Table of Contents

List of Figures

List of Tables

1. Introduction

1.1. Background and motivation

The demand for high-energy-density batteries continues to grow, driven by the rise of electric vehicles (EVs), renewable energy storage, and portable electronics. Traditional lithium-ion batteries (LIBs) face challenges in meeting future energy needs as they reach their fundamental performance limits. To address these shortcomings, lithium metal batteries (LMBs) have gained significant attention due to their high theoretical capacity, achieved by replacing the anode from graphite to lithium metal.[1] This could double the battery's energy density, enabling longer lasting and more compact, lightweight batteries. However, the practical use of lithium-metal batteries requires innovative approaches to overcome safety and stability challenges.

Polymer electrolytes are emerging as a key solution for LMB instability. The polymer electrolyte serves as the ionic conductor and the separator, removing the need for a liquid electrolyte. One of the most critical challenges in lithium-metal batteries is the formation of dendrites, which are needle-like structures that form on the lithium-metal anode.[2] Polymer electrolytes can address this issue by providing a mechanically robust matrix that suppresses dendrite growth.

Single-ion polymer electrolytes (SIPEs) are a specialized class of polymer electrolytes designed to address some of the limitations of traditional polymer-based ionic conductors. The polymer matrix is chemically modified in these materials to tether the anion covalently or via strong ionic interactions, leaving the cation (i.e., lithium in LIBs or LMBs) to move within the polymer matrix.[3] This single-ion conductivity approach eliminates the problem of anion-cation transference, a common issue in conventional polymer electrolytes where both ions contribute to conductivity but can result in inefficient ion transport and concentration polarization.[3]

Due to their distinct advantages in ionic conductivity and stability, SIPEs are regarded as highly promising candidates for LMBs. The successful implementation of this technology could greatly enhance the performance and reliability of applications such as EVs and portable electronics, addressing current energy storage challenges by enabling safer, more efficient, and higher-energy-density power solutions.

1.2. Research objectives

The primary objective of this research is to develop a lithium sulfonate-based polymer electrolyte and evaluate its potential for application in lithium metal batteries. This thesis is divided into four primary aims:

a. Synthesize a random copolymer (RCP) of PLSS and PEGMA with a wide range of monomer compositions to observe the structure-property relationship. Consider the number of ethylene oxide repeat units to lithium-ion ratios (EO:Li+) to ensure the most optimal ratio is found.

b. Fully characterize properties of PEGMA-*r*-PLSS copolymers and fabricate solid polymer electrolytes from these RCPs. Investigate chemical properties (e.g., chemical structure, composition, purity, molecular weight (MW)) to confirm successful synthesis. Investigate thermal properties (e.g., thermal degradation, glass transition temperature) and electrochemical properties (e.g., ionic conductivity) to establish suitability for LMB application and elucidate structure-property relationships.

c. Synthesize single-ion conducting polymer poly(lithium vinyl sulfonate) (PLVS) and perform full property characterization. Dope PEGMA-*r*-PLSS copolymers with PLVS to observe the impact on conductivity and film-forming properties.

d. Synthesize a series of block copolymers analogous to PEGMA-*r*-PLSS copolymers to compare block and random copolymers.

2. Literature review

2.1. Lithium-ion batteries

With the increasing issue of climate change, there is a high demand for clean and renewable energy. However, the effective storage of renewable energy remains a significant problem. Lithium-ion batteries (LIBs) have become the dominant energy storage solution in various applications, such as handheld electronics, laptops, and especially electric vehicles (EVs). This is due to their relatively high energy density, long cycle life, and efficiency.[4] However, LIBs still have a significantly lower energy density than other energy sources. While LIBs can store around 150-250 Wh/kg, gasoline contains approximately 13,000 Wh/kg.[5] This makes the energy stored in batteries considerably lower for the same weight. This energy density gap poses challenges, such as in sectors like transportation. Higher energy densities are needed for longer driving ranges and improved performance. As the demand for EVs continues to rise, the limitations of LIBs are becoming more pronounced. As seen in Figure 2.1, the demand for LIBs is expected to more than double by 2030, with EVs accounting for over 80% of the market.[4] Researchers are focusing on developing next-generation batteries, including lithium metal and solid-state batteries, offering higher energy densities to meet this demand. This can close the gap with traditional fossil fuels and enable more widespread adoption of electric-powered systems.

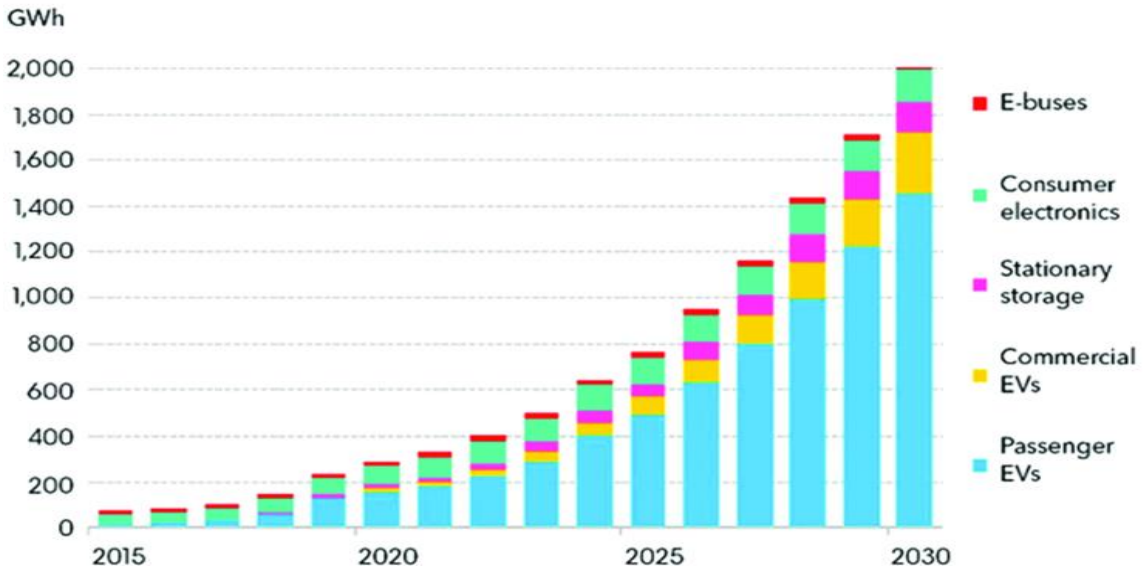

Figure 2.1 Annual growth of lithium-ion batteries. Reprinted with permission from [4]

2.2. Lithium metal batteries

With LIBs reaching their fundamental limits, other options must be explored. This has led to a reemergence of interest in lithium metal batteries (LMBs), where lithium metal is utilized for the battery's anode, replacing traditional graphite.[6–8] LMBs have emerged as one of the most promising energy storage technologies for next-generation applications, offering significant advantages over conventional LIBs. Lithium's high theoretical capacity and low weight could significantly enhance the overall battery's energy density. This makes LMBs attractive for applications where energy density and weight are critical factors, such as electric vehicles (EVs). However, the commercialization of LMBs faces several critical challenges, primarily related to safety and longevity.

Lithium metal batteries operate by using lithium metal as the anode, which provides a much higher specific capacity than conventional graphite anodes used in LIBs. The theoretical capacity of lithium metal is ~3,860 mAh/g, which is more than ten times higher than that of graphite (372 mAh/g).[9] In addition, lithium metal has the lowest electrochemical potential (-3.04 V vs. the standard hydrogen electrode), making it ideal for achieving higher cell voltages and improving the overall energy density of the battery.[1] Overall, all these factors could more than double the battery's energy density.

The basic operating principle of LMBs is similar to that of LIBs. During discharge, lithium ions move from the anode (lithium metal) to the cathode through the electrolyte, generating an electric current.[10] During charging, lithium ions return to the anode, where they are deposited as lithium metal. The ability to deposit and strip lithium metal during each charge and discharge cycle is key to the performance of LMBs. However, using current liquid electrolytes with lithium metal poses safety issues, primarily due to the formation of dendrites and consequent flammability issues.[6–8]

2.2.1. Dendrite formation and safety risks

Dendrite formation is one of the most critical issues facing LMBs and poses significant safety and long-term performance challenges. Dendrites are tree-like structures that form on the surface of the lithium metal anode during repeated charge and discharge cycles.[11] These dendritic structures grow and can eventually penetrate through the electrolyte and separator, leading to internal short circuits if they reach the cathode. A visualization of this dendrite formation can be seen in Figure 2.2. This causes the battery to fail and creates a severe safety risk since it can trigger thermal

runaway, which could lead to the battery catching fire or even exploding. The growth of dendrites also contributes to the continuous loss of active lithium, reducing the efficiency and capacity of the battery over time.[11]

The highly reactive nature of lithium metal, especially in contact with conventional liquid electrolytes, poses a significant safety risk. The reaction between lithium metal and the electrolyte can lead to the formation of flammable gases, increasing the potential for fire hazards.[10] LMBs tend to have a shorter cycle life compared to LIBs. Since lithium metal is being removed and readded during cycling, this leads to an uneven lithium distribution, loss of active lithium, and increased internal resistance.[10] Eventually, these effects degrade the battery's performance and limit its lifespan over time.

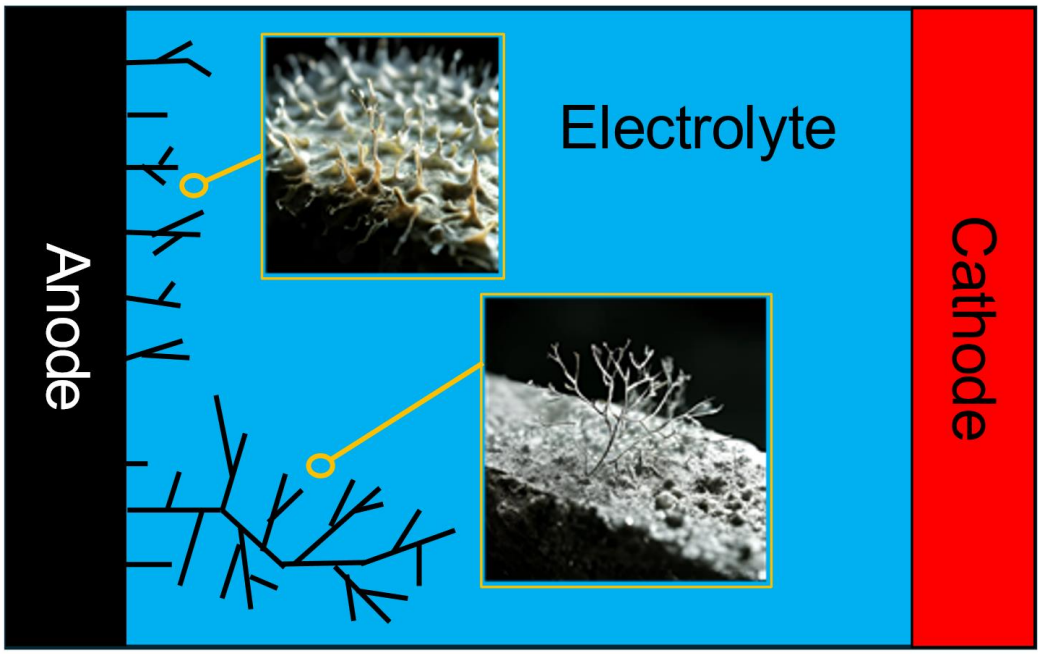

Figure 2.2 Visualization of dendrite formation. Images generated using Janus-Pro-7B[12]

2.3. Solid polymer electrolytes

To mitigate safety risks, there has been a transition toward solid-state batteries, where solid polymer electrolytes (SPEs) replace liquid electrolytes. Solid-state batteries offer improved safety and higher energy density, addressing the limitations of existing battery technologies.[6–8] Polymer electrolytes have gained significant attention for their potential use in advanced energy storage

systems, particularly in LMBs. Polymer electrolytes offer distinct advantages over liquid electrolytes, including better lithium dendrite blocking, improved safety and thermostability, and lower flammability. Unlike traditional liquid electrolytes, where salts are dissolved in organic solvents, polymer electrolytes incorporate lithium salts directly into a polymeric structure. This solid or semi-solid matrix allows the transport of lithium ions while simultaneously providing structural integrity.

2.3.1. Key properties of polymer electrolytes

Polymer electrolytes possess several key properties that make them essential for LMBs. One of the most important characteristics is ionic conductivity, which refers to the ability of lithium ions to migrate through the polymer matrix under an applied electric field, a critical factor in determining the battery's overall efficiency. The polymer must also have good mechanical properties (i.e., shear modulus) to stop dendrite formation. SPEs must have a shear modulus twice that of lithium metal to prevent dendrite formation.[13] Another advantage of SPEs is their flexibility and processability, allowing them to be manufactured into thin films or coatings for various battery designs.[14] This allows for more scalability for real-world applications. By modifying the polymer backbone or introducing specific functional groups, polymer electrolytes can be tailored to achieve various conductivities and mechanical properties, optimizing their performance in different battery systems.

Polymers for SPEs must have a low glass transition temperature (T_g) to allow for the polymer to be in a more flexible state.[15] This flexibility allows for more free volume between polymer chains, which allows the lithium ions to move much more freely, increasing conductivity. Additionally, high thermal stability is crucial for preventing electrolyte breakdown and cell failure.[16] Thermal stability is also important for the polymer electrolyte since the battery may heat up during cycling. This allows the battery to remain operational in extreme conditions and increases safety, preventing a thermal runaway.

Other critical properties of SPEs are the electrochemical stability window (ESW) and the lithium transference number. ESW refers to the voltage range within which an electrolyte remains stable without undergoing oxidation or reduction.[17] A wider ESW is desirable, as it allows the use of higher energy-density materials (e.g., high-voltage cathodes or lithium metal anodes) and contributes to the overall safety and longevity of the battery. The Li^+ transference number is a key

parameter in evaluating the performance of electrolytes in both LIBs and LMBs. It represents the fraction of the total ionic current carried by lithium ions (Li^+).[18] For single ion conducting polymers, the ideal lithium transference number would be 1, meaning that the lithium ions would carry all the current.

2.3.2. Types of polymer electrolytes

There are three main types of polymer electrolytes: solid polymer electrolytes (SPEs), gel polymer electrolytes, and hybrid polymer electrolytes. SPEs typically contain a lithium salt dissolved in the polymer, which is typically a polyethylene oxide (PEO) based polymer. Though SPEs have strong mechanical properties which are effective in stopping dendrites, they suffer from low conductivity, with many falling from 10^{-7} to 10^{-5} S cm^{-1} at room temperature.[19] At higher temperatures, they often see an increase in conductivity. Gel polymer electrolytes are similar to SPEs; however, a small amount of liquid electrolyte increases their conductivity to ~10^{-3} S cm^{-1} at room temperature.[20] This increase in conductivity helps with the battery's performance but compromises the mechanical stability. This also leads to safety issues due to the flammability of the liquid electrolyte. The last option, the hybrid polymer electrolyte, involves a polymer matrix mixed with another material, such as ceramics or other organic particles.[21] Combining these two materials can provide good conductivity, but it is still limited compared to liquid electrolytes. This project will mainly focus on SPEs.

SPEs also have their own drawbacks compared to liquid electrolytes. Mainly, their ionic conductivity is much lower than liquid electrolytes. Liquid electrolytes have the highest conductivities, often several orders of magnitude higher than polymer electrolytes. The most common electrolyte used for LIBs is lithium hexafluorophosphate ($LiPF_6$) which has a conductivity in the range of 5×10^{-3} to 1.5×10^{-2} S cm^{-1} at room temperature compared to most polymer electrolytes at 10^{-7} to 10^{-5} S cm^{-1} at room temperature.[22] Another drawback of SPEs is the trade-off between the necessary mechanical properties and the desired electrochemical properties. Increasing the electrochemical properties often results in insufficient mechanical properties to completely stop the dendrite formation. However, the electrochemical properties should be optimized first when designing a polymer electrolyte. Then, the polymer structure can be modified to introduce mechanical properties that will be viable for stopping dendrite formation. The ESW is often lower in polymer electrolytes than that of liquid electrolytes. This can potentially

restrict the battery's operating voltage and prevent the use of certain electrode materials that require a certain ESW. Also, certain polymer electrolytes may react with lithium metal, which can cause chemical degradation of the polymer, reducing overall performance. Ongoing research into novel polymer designs aims to overcome these challenges and improve the performance of polymer electrolytes.

2.3.3. Dual-ion polymer electrolytes

SPEs typically contains a polymer matrix dissolved with a lithium salt. This is known as a dual-ion polymer electrolyte (DIPEs). The salt usually includes a strong withdrawing electron anion and the lithium cation.[23] Due to several advantageous properties, the most common salt used is Lithium bis(trifluoromethane sulfonyl)imide (LiTFSI). LiTFSI synergizes well with polymer matrices such as PEO since the ions can easily dissociate, creating high concentrations of lithium ions.[24] This allows the lithium ions to move freely along the polymer chains, increasing the conductivity. The (trifluoromethanesulfonyl)imide (TFSI) anion also helps reduce the crystallinity of PEO, creating more amorphous regions and enhancing ionic conductivity.[24] TFSI will also help with ionic conductivity by carrying some of that charge.

2.4. Single-ion polymer electrolytes

The primary type of polymer electrolytes discussed herein are SIPEs, where the lithium cation is the sole charge carrier. At the same time, the anion is covalently attached to the polymer structure and remains stationary.[3] This design aims to remove the migration of negatively charged anions, which would otherwise contribute to concentration gradients, decreased ionic conductivity, and inefficiencies during battery operation. By restricting the movement of anions, single-ion conducting electrolytes create a more stable environment for lithium-ion transport, improving overall performance.[25]

2.4.1. Single-ion polymer electrolytes versus dual-ion polymer electrolytes

SIPEs offer many advantages over DIPEs, which often lie in their selective mobility of lithium ions. Since only the lithium-ion is being transported, SIPEs often have reduced polarization, meaning lithium ions will have a better, more even distribution.[3] In dual-ion polymer electrolytes, the anion and the cation migrate throughout the electrolyte. This can create uneven concentration gradients or regions in the electrolyte with a highly concentrated area of lithium ions or anions. This will hinder the conductivity and eventually impede the battery's overall performance. SIPEs

eliminate this issue, resulting in more uniform lithium-ion distribution. Table 2.1 shows the difference in structure comparing DIPEs and SIPEs.

Table 2.1 Comparison of the structure of dual-ion polymer electrolytes (DIPEs) and single-ion polymer electrolytes (SIPEs). Adapted from [26]

Feature	Dual-Ion Polymer Electrolytes (DIPEs)	Single-Ion Polymer Electrolytes (SIPEs)
Charge Transport	Both cations and anions contribute	Only one ion (usually cation (Li^+) moves
Electrochemical Stability	Moderate to high, depending on ion pairing	Typically, higher due to fixed counter-ion
Polymer Matrix Role	Dissolves both ions for transport	Immobilizes counter-ion, allowing single-ion conduction

Lithium transference number, t_{Li+}, is the fraction of the total current carried by lithium ions and is an important metric for SIPEs. In conventional DIPEs, the t_{Li+} is typically between 0.2 and 0.4, because lithium ions and anions contribute to the ionic current.[27] For SIPEs, a higher t_{Li+} (i.e., close to 1) is expected.[18] This is a key advantage to SIPEs, enabling more efficient charge-discharge cycles and better performance in lithium metal batteries.

SIPEs can also lead to improved cycle life and stability relative to DIPEs, where the migration of both lithium ions and anions can lead to side reactions with the electrodes, especially with the reactive nature of lithium metal, degrading the electrolyte and electrodes over time.[28] The mobile anions are the main issue of this degradation; when decomposed, they create toxic materials from the side reactions that can cause damage. One example is $TFSI^-$ anion; it can generate fluorinated by-products such as hydrofluoric acid upon decomposition.[29] Hydrofluoric acid is highly corrosive and can damage all battery components. In contrast, lithium ions have been proven to be stable and compatible with common battery materials. SIPEs eliminate the negative effects of mobile anions by limiting ionic transport to Li^+.

2.4.2. Single-ion polymer electrolyte ion transport mechanism

The ion transport mechanism in SIPEs fundamentally differs from that in conventional polymer electrolytes. In dual-ion systems, an electric field drives lithium ions and anions through the electrolyte. In SIPEs, only the lithium ions move along the polymer chains in a “hopping” mechanism.[30] Lithium ions move along the polymer chains and jump to the next chain when needed. A visualization of this interchain and intrachain hopping can be seen in Figure 2.3. PEO

is an ion-conducting, semi-crystalline polymer with both amorphous and crystalline regions, where ion conductivity mainly occurs in the amorphous regions.[31] PEO-based polymers are widely used for this application since they create coordination sites for the lithium ions.[30] The oxygen atoms in PEO interact with the lithium ions, creating pathways for ion transport. Lithium ions bind to these oxygen atoms to form a stable, but not permanent, interaction. This relatively weak binding allows lithium ions to move between coordination sites. The lithium-ion hopping mechanism is much more efficient in the amorphous regions of PEO due to more free volume and pathways for the lithium ions. Higher temperatures can also make the hopping mechanism much more effective since it will increase the segmental motion in the polymer chains, especially in the amorphous regions.

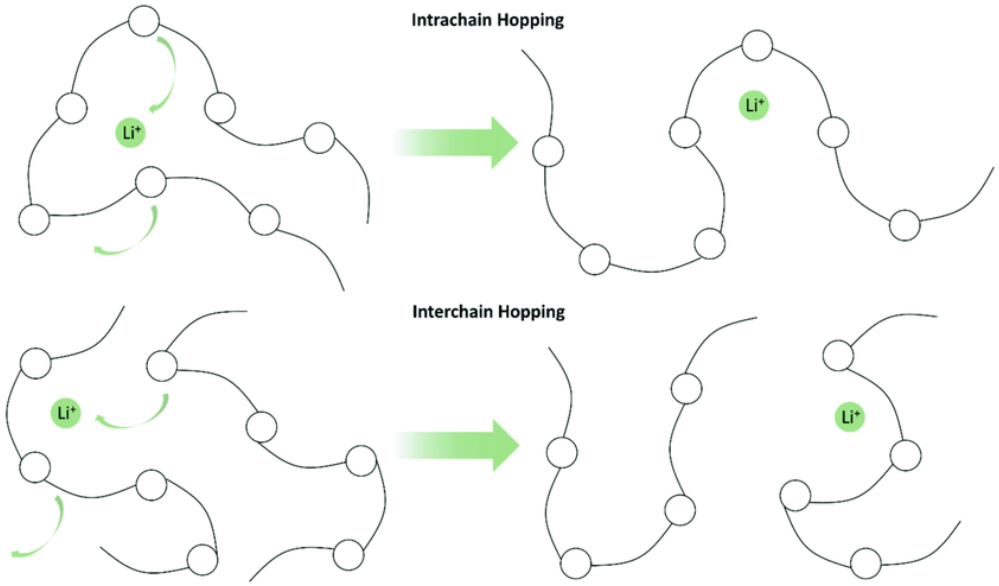

Figure 2.3 Ion transport mechanism. Reprinted with permission from[30]

2.4.3. Effect of polymer structure on ionic conductivity

PEO has been a well-studied polymer electrolyte system due to its high segmental motion and low glass transition temperature.[32] However, PEO crystallinity increases above ~60°C, which reduces its ionic conductivity. For DIPEs, the TFSI anion mitigates the crystallinity of PEO, but in SIPEs, there is no TFSI anion. Another polymer, poly(ethylene oxide) methyl ether methacrylate (PEGMA), has been studied to overcome this crystallinity.[32] The structure of PEGMA contains the PEO structure; however, this PEO is not in the polymer backbone. Instead, PEGMA contains a methacrylate group on the backbone, with a long PEO chain attached to it, reducing the polymer's

ability to organize into a regular, crystalline lattice and resulting in a generally amorphous material. This amorphous structure provides greater chain flexibility and free volume, creating better movement pathways for ions.

2.4.4. Different delocalizing anions for single-ion polymer electrolytes

Since SIPEs contain a strong electron-withdrawing group in the polymer structure, it must be incorporated in a way that does not limit the conductivity of the electrolyte. The most common polymer backbone for incorporating a covalently tethered, strong electron-withdrawing anion is polystyrene (PS). Polystyrene is cheap, has facile synthesis, and has a benzene ring structure that readily accommodates substitutions, making it easy to functionalize with a strong electron-withdrawing anion. PS has desirable mechanical properties, which provide a tough and durable framework that reinforces the electrolyte structure without compromising its overall flexibility. One drawback of both PEO and PEGMA is their poor mechanical strength, which can be improved by copolymerizing them with PS.[6–8,32] Since PS is also amorphous due to its bulky benzene rings, it can provide mechanical properties without greatly hindering ionic conductivity.[6–8,32]

Substitutions on polystyrene improve the polymer's ion-conducting properties while maintaining mechanical strength. Since polystyrene can accommodate many different groups, there are many options.[33] These groups create polar microenvironments within the polymer matrix that help stabilize cations by coordinating with them and facilitating the movement of free ions (e.g., Li^+) through the electrolyte. The general trend is that more electronegative groups will increase ionic conductivity.[3] Since the TFSI anion was found to work well in DIPEs, similar electron-withdrawing groups were added to polystyrene in literature to create a similar effect.[34] Increasing the electronegative effect of the covalently attached anion was found to increase ionic conductivity slightly, and even more electronegative groups than TFSI were found to increase conductivity even further.[35] Figure 2.4 shows some examples of the delocalizing groups that can be attached to PS.

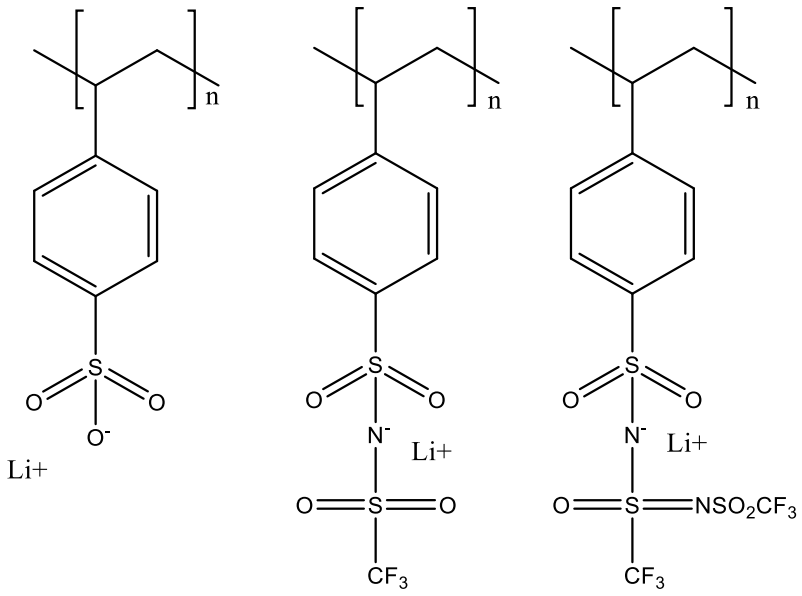

Figure 2.4 Examples of SIPEs based on polystyrene. Adapted from [35]

It should be noted that functionalizing PS with TFSI groups can require complex synthesis procedures, often requiring multiple steps under challenging conditions. For example, the polymer on the right in Figure 2.4 requires a long series of steps, which also require synthesis in an inert argon atmosphere in a glove box.[36] Each step results in material losses, and optimizing each step to move to the next step is a complex and lengthy process. From an engineering perspective, this makes it less likely that these polymers can be produced economically at an industrial scale, even if their electrochemical properties are satisfactory. In contrast, sulfonated PS (Figure 2.4 left) is being produced on an industrial scale and still has relatively high conductivity at room temperature (i.e., $>10^{-8}$ S cm^{-1}, versus that of TFSI attached to PS (Figure 2.4 middle), which has a conductivity of $>10^{-7}$ S cm^{-1} at room temperature.)[33,37]Table 2.2 shows some possible anionic centers desirable for this application and their respective properties.

Table 2.2 Different anionic centers and their respective conductivities. Adapted from [6]

Anionic center	Type of electrolytes	Conductivity (σ) S cm^{-1}
$–CO_2^-$	Blend polymer	1.5×10^{-7} (25 °C)
$–CO_2^-$	Random copolymer	2.0×10^{-7} (25 °C)
$–CO_2^-$	Block copolymer	10^{-7} (25 °C)
$–(CF_2)_3CO_2^-$	Blend polymer	10^{-8} (25 °C)
$–SO_3^-$	Blend polymer	1.8×10^{-7} (25 °C)
$–SO_3^-$	Random copolymer	2.0×10^{-7} (25 °C)
$–CF(CF_3)SO_3^-$	Random copolymer	10^{-7} (25 °C)
$–C_6H_5SO_3^-$	Blend polymer	3.0×10^{-8} (25 °C)
$–C_6H_5SO_3^-$	Random copolymer	1.5×10^{-7} (30 °C)
$–COCF_2SO_2N^{(-)}–$	Blend polymer	10^{-6} (100 °C)
$–COCF(CF_3)O(CF_2)_2SO_2N^{(-)}–$	Blend polymer	10^{-5} (30 °C)
$–SO_2(CF_2)_4SO_2N^{(-)}–$	Blend polymer	10^{-6} (25 °C)
$–SO_2N^{(-)}SO_2CF_3$	Blend polymer	10^{-9} (25 °C), 10^{-6} (60 °C)
$–SO_2N^{(-)}SO(NSO_2CF_3)CF_3$	Blend polymer	10^{-8} (25 °C), 10^{-5} (60 °C)
$–SO_2N^{(-)}SO_2F$	Blend polymer	10^{-8} (25 °C), 10^{-5} (60 °C)
$–SO_2N^{(-)}SO_2CF_3$	Random copolymer	3.0×10^{-6} (25 °C)
$–SO_2N^{(-)}SO_2CF_3$	Random copolymer	7.7×10^{-6} (25 °C), 10^{-4} (60 °C)
$–SO_2N^{(-)}SO_2CF_3$	Triblock copolymer	1.3×10^{-5} (60 °C)
$–SO_2N^{(-)}SO_2CF_3$	Block copolymer	2.3×10^{-6} (25 °C), 10^{-5} (70 °C)

2.4.5. Ethylene oxide to lithium-ion ratio

In SIPEs with repeat ethylene oxide (EO) units, there is an essential balance between the ratio of EO repeat units to lithium ions in the electrolyte ([EO]/[Li^+]).[38] Too many EO repeat units (i.e., too many coordination sites for lithium) will cause low ionic conductivity and sluggish ion transport, adversely affecting battery performance.[38] Having too many lithium ions means there will not be enough coordination sites for the lithium ions, which causes the electrolyte to exhibit poor ion dissociation, low ionic conductivity, and potentially higher resistance, degrading the battery's efficiency and capacity. The optimal [EO]/[Li^+] ratio based on literature has been found to be around 9:1.[37] Having too high or too low of a [EO]:[Li^+] ratio will directly contribute to a lower conductivity, and new materials should be evaluated across a range of ratios since changing the overall polymer structure may affect the optimal ratio.

2.5. Balancing ionic conductivity with mechanical properties

SPEs for battery applications require high ionic conductivity. Polymers with flexible properties or amorphous structures generally have better ion mobility and conductivity. However, they are often much more mechanically weak. Achieving optimal ionic conductivity without compromising mechanical integrity is difficult. One way to improve the mechanical properties of a SPE while maintaining conductivity is to incorporate crosslinking into the polymer structure, making it less prone to mechanical stress. Crosslinking can be achieved chemically or physically by adding crosslinking agents via radiation or heat treatment.[39] However, too much crosslinking can cause a decrease in flexibility, therefore dropping ionic conductivity. Adding inorganic nanoparticles, such as silica (SiO_2), alumina (Al_2O_3), or titanium dioxide (TiO_2) can enhance the mechanical properties as well.[40–42] These nanoparticles act as fillers that improve the structural integrity and stability of the polymer matrix. For instance, adding TiO_2 nanoparticles has improved mechanical strength and ionic conductivity.[40] Other inorganic fillers have seen a similar effect, improving mechanical strength and contributing to better electrochemical performance.[42]

Another way to balance conductivity and mechanical properties is to combine a conductive polymer with a mechanically reinforcing polymer, either by directly blending the two polymers or by synthesizing a copolymer of the two monomers, such as a block or random copolymer.

2.5.1. Block copolymers versus random copolymers

Polymers with dual properties are highly desirable for SIPE applications and can be effectively created via block copolymers (BCPs) and random copolymers (RCPs). RCPs contain two or more monomers added during synthesis, leading to a random monomer distribution along the polymer backbone, while BCPs contain distinct segments of each monomer in a block-like structure.[43] As a result, RCPs have a more uniform and homogenous structure with averaged properties of the monomers, while BCPs exhibit phase separation, leading to heterogeneous properties that reflect the distinct characteristics of each monomer (e.g., electrochemical, mechanical).

Both configurations have advantages. BCPs have potentially higher ionic conductivity since phase separation allows for forming continuous ion-conducting domains, improving lithium-ion transport.[44] Due to their distinct phase separation, BCPs have also been found to display better properties for stopping dendrites.[43] Despite their merits, BCPs often require more synthesis steps

and may have lower processability relative to RCPs.[45] As a result, RCPs have more advantageous procedures that are scalable to industry.

2.5.2. Block copolymer synthesis techniques

Block copolymers are commonly synthesized using controlled polymerization techniques, such as atom transfer radical polymerization (ATRP) or reversible addition-fragmentation chain transfer (RAFT) polymerization.[43,46] These techniques allow precise control over the molecular weight (MW) of the overall polymer and the number of repeat units of each block. Typically, BCPs have a low polydispersity index (PDI) (i.e., narrow MW distribution), allowing for consistent mechanical and electrochemical properties.[43,46] For battery applications, a BCP could be synthesized via the sequential addition of mechanical and electrochemical blocks and processed into thin films after synthesis to be used as a solid-state electrolyte (SSE).

2.5.3. Random copolymer synthesis techniques

Random copolymers are typically synthesized using free radical polymerization, which is efficient, versatile, and cost-effective.[47] In free radical polymerization, two or more monomers are copolymerized in a single reaction, resulting in a polymer chain with a random distribution of the different monomer units.[48] While RCPs typically have higher MW distributions (PDI ~2), controlled radical polymerization methods, such as ATRP and RAFT polymerization, can also be used to synthesize RCPs of more consistent MWs and controlled compositions, allowing for more consistent final properties.[49] For battery applications, two monomers (i.e., mechanical and electrochemical) can be reacted simultaneously, allowing for their random incorporation along the polymer chain. This results in an RCP that is more easily processed into a thin-film solid-state electrolyte.

2.6. Performance metrics

Performance metrics for SIPEs for LMBs are critical for assessing their capability to perform and operate in a battery effectively. Ionic conductivity is the most important, as high conductivity enables rapid lithium-ion movement across the electrolyte. In LMBs, SIPEs should reach at least 10^{-4} to 10^{-3} S/cm at room temperature to support fast charging and high-power applications.[3] Lithium transference number is particularly significant for SIPEs, designed to suppress anion movement entirely, and ideally, it would be nearly 1.[18] A high lithium transference number is essential for sustaining stable, high-efficiency cycling, whereas a low lithium transference number

can lead to reduced efficiency and electrolyte degradation.[50] This could also cause an increase in polarization with a higher concentration of lithium ions residing near the electrodes rather than being in the bulk of the electrolyte. The ESW is also critical to ensure compatibility with the lithium metal anode. SIPEs need a stability range of up to 4.5 V to withstand high-voltage cathodes without decomposing or reacting with lithium.[27] Mechanical properties are also important to stop dendrite formation; therefore, the shear modulus must be twice that of lithium metal. SIPEs should demonstrate good thermal stability, tolerating high temperatures while maintaining flexibility for effective interfacial contact with electrodes. Together, these metrics support the development of SIPEs that enhance safety, conductivity, and durability in LMBs.

3. PEGMA-*r*-PLSS random copolymers for lithium metal batteries

3.1. Introduction

Developing advanced materials for LMBs is crucial to achieving higher energy densities and improved safety in next-generation energy storage systems. However, rechargeable LMBs suffer from dendrite formation, a tree-like structure that forms on the lithium anode during the recharge cycle, causing the battery to short circuit, which can lead to fires or even explosions.[51] Solid-polymer electrolytes (SPEs) offer a promising solution to the dendrite formation problem in batteries by providing a stable, rigid structure that physically blocks dendrite growth, enhancing both safety and cycle life by preventing short circuits and maintaining uniform ion transport. One promising class of materials gaining attention for application as SPEs in LMBs is random copolymers, which can offer tailored properties by combining different monomer units. Among these, PEGMA-*r*-PLSS random copolymers have high potential as candidates for enhancing the performance of LMBs.

While PEO is a commonly used polymer for battery applications, it is known to face performance limitations at temperatures below 60-70ºC, where its increased crystallinity reduces ionic conductivity, and hinders the material's mechanical flexibility and overall cycle stability.[52] Lower temperatures (e.g., room temperature, ambient temperature) are of high interest for battery applications, making PEGMA an optimal replacement for PEO, as it also contains flexible EO units but as side chains rather than in the polymer backbone, thus it has an amorphous structure.[32] These bulky EO side chains similarly provide flexibility and facilitate ion transport, while improving ionic conductivity at ambient temperatures.

PEGMA lacks mechanical properties for stopping dendrites and does not contain a site for lithium ions required for a single-ion conductor, thus requiring a copolymer. Due to its strong ionic nature, PLSS was considered a complementary component in this system. The sulfonate groups on PLSS allow for the lithium ions to be incorporated into the polymer structure as a single-ion conductor. PLSS, as a homopolymer, reaches high ionic conductivities of $>10^{-8}$ S cm^{-1} at room temperature and $>10^{-7}$ S cm^{-1} at higher temperatures.[37] Additionally, the rigidity of the polystyrene backbone offers structural stability, which is needed to stop dendrite formation.

In this study, the single ion conducting random copolymers, PEGMA-*r*-PLSS, were investigated as a function of ionic composition to explore the relationship between ion conductivity, glass transition temperature, and EO:Li^+ ratio. Thus, the RCP was synthesized at various PLSS compositions from 12% to 75% via reversible addition−fragmentation chain transfer (RAFT) polymerization. The thermal properties and ion conductivity of these SPEs were investigated in this study. The composition of the copolymer, where PLSS contains Li^+ and provides mechanical properties, while PEGMA contains EO coordination sites for the lithium ions to transport, was balanced to observe a synergistic effect whereby the desired properties for LMBs (i.e., having both a free-standing solid polymer electrolyte and high ionic conductivity) were achieved.

3.2. Experimental

3.2.1. Materials.

Deuterium oxide (D_2O, ≥99.9%) was purchased from Cambridge Isotope Laboratories. All other chemicals were purchased from Sigma-Aldrich and used as received unless otherwise noted. Poly(ethylene glycol) methyl ether methacrylate (PEGMA) with an average Mn of 500 was purified with an inhibitor-remover column to remove the Mequinol (MEHQ) inhibitor. Sodium 4-vinyl benzenesulfonate was purchased from Sigma Aldrich. The initiator 2,2′-azobis-(isobutyronitrile) (AIBN) was purchased from Sigma Aldrich and recrystallized twice from methanol before use. Lithium hydroxide monohydrate (LiOH, 99.0%) was purchased from Sigma Aldrich. N,N- dimethylformamide (DMF, ACS Reagent, ≥99.8%) was purchased from Fisher Scientific. Dimethylsulfoxide (DMSO, ACS Reagent, ≥99.9%) was purchased from Fisher Scientific. The chain transfer agent 2-cyano-2-propyl dodecyl trithiocarbonate was purchased from Sigma Aldrich.

3.2.2. Synthesis of PEGMA-r-PSS.

The synthesis of random copolymer PEGMA-*r*-PSS was based on the work of Wang et al.[32] All copolymers were synthesized by reversible addition−fragmentation chain transfer (RAFT) polymerization in solution. A dry glass reactor with a magnetic stir bar was charged with PEGMA, sodium styrene sulfonate (NaSS), 2-cyano-2-propyl dodecyl trithiocarbonate (RAFT chain transfer agent, CTA), AIBN, and 30 mL of dimethylformamide (DMF) to achieve 0.1 M monomer concentration.[32] The RAFT agent and AIBN were at a 5:1 molar ratio respectively, with their total being 1.5 mol% of the total monomers. Before the reaction, three freeze−pump−thaw cycles were

applied to the reactant solution with liquid nitrogen under vacuum to remove oxygen and moisture from the reaction chamber. The reaction was maintained at 80°C for 24 hr under nitrogen.[32] Unreacted monomers and lower MW polymers were removed by dialysis with deionized water (DIW) using a Slide-A-Lyzer G2 dialysis cassette with a 3500 MW cutoff with a 70 ml sample size. The reaction product was first quenched with liquid nitrogen. The mixture was then thawed and added to the dialysis cassette, and the remaining space was filled with DIW. The cassette was immersed in a 4 L beaker filled with DIW while the dialysate was changed with DIW every 2 to 4 h for roughly 10 hours total. The DMF from the synthesis was removed quickly during dialysis and was not found to damage the dialysis membranes. The solution was removed from the cassette tape, and the excess DIW was removed using a rotary evaporator. The remaining concentrated solution was then vacuum-dried at 80 °C for 24 h. The yield of the final product after dialysis was approximately 40–50%. The synthesis procedure and ion exchange metathesis can be seen in Figure 3.1.

3.2.3. Ion Exchange Metathesis to PEGMA-*r*-PLSS.

The synthesized copolymers were ion-exchanged from sodium to lithium. First, the PEGMA-*r*-PSS copolymers were dissolved in dimethyl sulfoxide (DMSO) at 90°C.[53] Once dissolved $LiOH \cdot H_2O$ was added to the mixture in about a 10:1 ratio (mol Li^+: mol Na^+) and mixed for 24 h.[53] The amount of $LiOH \cdot H_2O$ added varied by the molar percentage of PSS in the copolymer. The excess salt was then removed using dialysis with DIW using a Slide-A-Lyzer G2 dialysis cassette with 2000 MW cutoff with 15 ml sample size. The cassette was immersed in a 4 L beaker with DIW while the dialysate was changed with DIW every 2 to 4 h for roughly 10 hours. The samples were then removed and vacuum-dried at 80°C for 24 h. The yield of the final product after ion exchange and dialysis was approximately 50-60%. The full synthesis procedure and ion exchange metathesis can be seen in Figure 3.1.

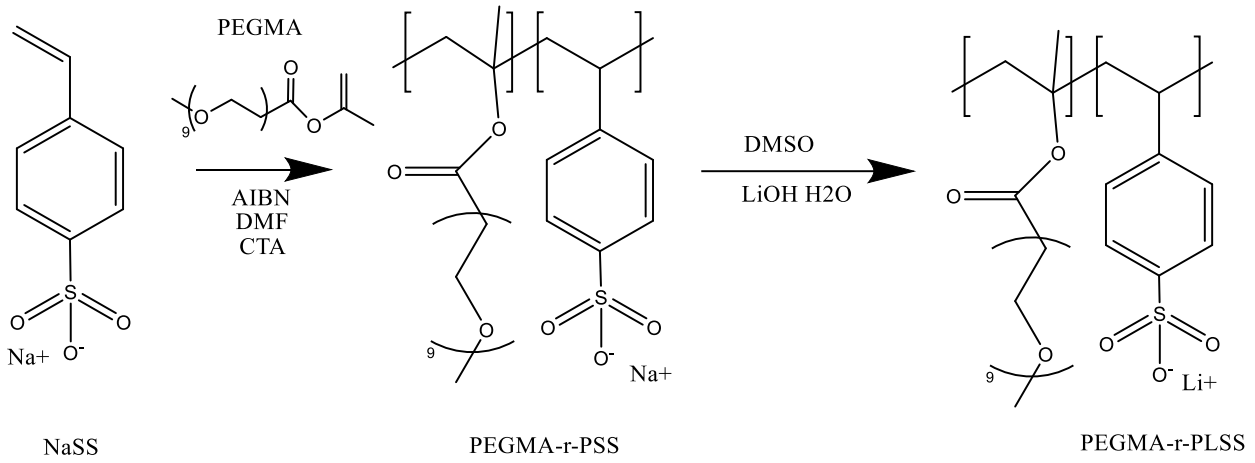

Figure 3.1 The synthesis procedure of PEGMA-r-PLSS

3.2.4. Polymer casting

Polymer samples were dissolved in DIW (5 or 10 wt% polymer, depending on solubility) and stirred overnight to ensure complete dissolution. The solution was then cast onto a Teflon sheet in a petri dish, covered with a glass funnel, and left ~2 days while the solvent evaporated. The funnel was removed, and the casts dried in ambient conditions for another 24 h. The casts were then placed in the vacuum oven, dried at 80 °C without vacuum for ~3 h, then dried under vacuum for 24 h. After drying, polymer films were removed from the Teflon as free-standing films.

3.3. Characterization.

3.3.1. Proton Nuclear Magnetic Resonance Spectroscopy (^{1}H NMR)

^{1}H NMR spectra were recorded on a Bruker Avance III 500 MHz with TOPSPIN software. D_2O (~1 mL) was used to dissolve ~5 mg of copolymer sample. Chemical structures were determined from the ^{1}H NMR spectra, with all peaks assigned and quantitatively understood.

3.3.2 Fourier-Transform Infrared Spectroscopy (FTIR)

FTIR spectra were recorded using Agilent Cary 630 FTIR Spectrometer. FTIR was used to confirm the success of the ion exchange between the sodium and lithium ions.

3.3.3. Gel permeation chromatography (GPC)

GPC was recorded using Thermal Scientific Ultimate 3000 HPLC to determine the MW of the polymer samples. The device was calibrated using polystyrene standard samples to ensure accurate MW. Due to their ionic properties, samples were run in DMF columns with 0.05 M lithium bromide (LiBr) at 35 °C with a flow rate of 1 mL/min.

3.3.4. Thermal Characterization

The copolymers' thermal behavior was observed by differential scanning calorimetry (DSC; TA Instruments, Q2000) over a temperature range of -90 to 180 °C at a heating/cooling rate of 10°C min^{-1} under an N_2 environment using a heat/cool/heat method. The glass transition temperature was analyzed by midpoint method using TA instruments Trios analysis software. Thermal degradation of the copolymers was measured by thermal gravimetric analysis (TGA; TA Instruments, Q550) using a temperature ramp to 900 °C at a heating rate of 10°C min^{-1} under an N_2 environment.

3.3.5. Electrochemical Characterization

The ionic conductivities of polymer films were measured with electrochemical impedance spectroscopy (EIS) over a frequency range of $10-10^6$ Hz at 10 mV. Six different points were taken at room temperature: 30, 40, 50, 60, and 70 °C. The conductivities of the polymer films were measured in a split cell (MTI split cell for R&D battery 15mm I.D.) with a two-electrode setup, where an alternating current was applied across the two electrodes, and the actual impedance or resistance, R, was determined from the measured voltage and current. The resistance was determined from the high x-intercept of the semicircle regression of the Nyquist plot using the EC-lab software. An example Nyquist plot can be seen in Appendix A.4. Conductivity was calculated using Equation 3.1,

$$\sigma = \frac{L}{AR} \qquad (Equation\ 3.1)$$

where L is the distance between electrodes, A is the cross-sectional area of the polymer film, and R is the resistance.

3.4. Results and Discussion.

3.4.1. Chemical Properties.

PEGMA-*r*-PSS was synthesized at seven different compositions and characterized via ^1H NMR. The copolymer compositions and monomer feed ratios are reported in Table 3.1. Figure 3.2 shows the labeled NMRs and PEGMA-*r*-PLSS chemical structure. The 4 protons on the benzene ring of PLSS can be seen in the peaks from 6.0 to 7.8 ppm, labeled as peak “a”. The prominent peak at ~3.6 ppm results from the ethylene oxide (EO) side chains on PEGMA, labeled peak “b.” Peak “c” represents the methyl group at the end of the PEGMA side chains at around 3.2 ppm. In the higher

percentage PEGMA samples, such as PEGMA-*r*-PLSS-12 and PEGMA-*r*-PLSS-26, a peak can be seen around 4 ppm, for protons on the (EO) side chains that are near the (C=O) bond on the methacrylate group.[54] These hydrogens may experience additional deshielding due to the combined effects of the C=O and the ether oxygen, shifting their resonance to higher ppm values.

Overall, the MW was in the range of around 5100-10900 g/mol. The variation mainly comes from the difference in molar mass of PSS (MM=206 g/mol) compared to PEGMA (MM=500 g/mol). When the copolymer composition is higher in PEGMA, it has a higher MW, so the highest MW at 10.9 kg mol^{-1} corresponds to the highest % PEGMA sample. The role of the CTA is to keep the number of repeat units constant, which causes the difference in MW. While not as uniform as polymers with a lower PDI, they still offer good consistency in their material properties, making them suitable for the desired application of batteries.

Table 3.1 Composition, synthesis recipe, and molar masses of PEGMA-r-PLSS copolymers from ^{1}H NMR and GPC

Copolymers	**PEGMA-*r*-PLSS composition (mol% PLSS)**	**Mol PEGMA: mol SS in synthesis**	**Molar ratio EO:Li^+ in PEGMA-*r*-PLSS**	**M_n (kg mol^{-1})**	**PDI**
PEGMA-*r*-PLSS-12	12%	4:1	66:1	10.9	1.4
PEGMA-*r*-PLSS-26	26%	2:1	25:1	7.7	1.8
PEGMA-*r*-PLSS-35	35%	1.67:1	17:1	-	-
PEGMA-*r*-PLSS-50	50%	1:1	9:1	5.1	1.4
PEGMA-*r*-PLSS-65	65%	0.5:1	4:1	5.6	1.6
PEGMA-*r*-PLSS-75	75%	0.33:1	3:1	-	-

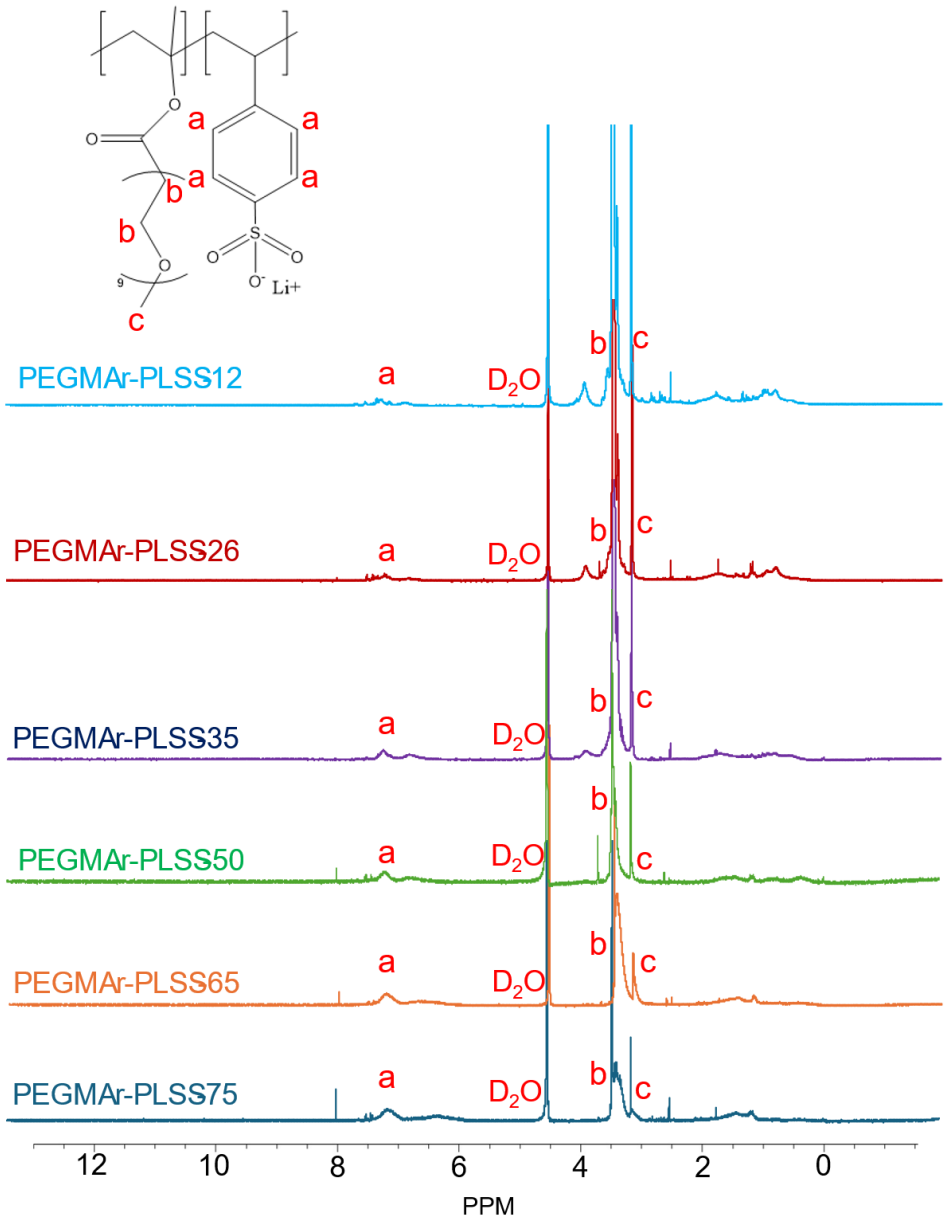

Figure 3.2 PEGMA-r-PLSS NMRs in Na+ form

Ion exchange metathesis was performed to exchange the copolymer to lithium-ion form for battery applications. Figure 3.3 below shows the FTIR spectra before and after the ion exchange. Based on the work of Park *et al.,* the characteristic peaks confirming the exchange of Na^+ in PSS to Li^+ in PLSS were assigned at ~1410 cm^{-1}, confirming that the ion exchange was successful.[37] Based on the different copolymer compositions, the higher percentage PLSS copolymers should have stronger peaks at these wavenumbers. Park *et al.* also attributed peaks at ~830 and ~1070 cm^{-1} to the sodium-to-lithium exchange; herein, these peaks are difficult to assign due to the copolymer

structure. The PEGMA portion has distinct peaks that overlap with many of PSS/PLSS, making it difficult to see new peaks that would show up during the ion exchange. A similar work by Kwon *et al*. showed that, in their case, there was no way to verify by FTIR that the ion exchange had occurred.[53] Therefore, having a distinct peak allows for qualitative analysis of whether the ion exchange was successful. It is also noted that there are two unique peaks at ~1600 cm^{-1}, most likely water, as water is also noted by the increase in the peak at ~3400 cm^{-1}. The appearance of the lithium peaks ensured the ion exchange was successful.

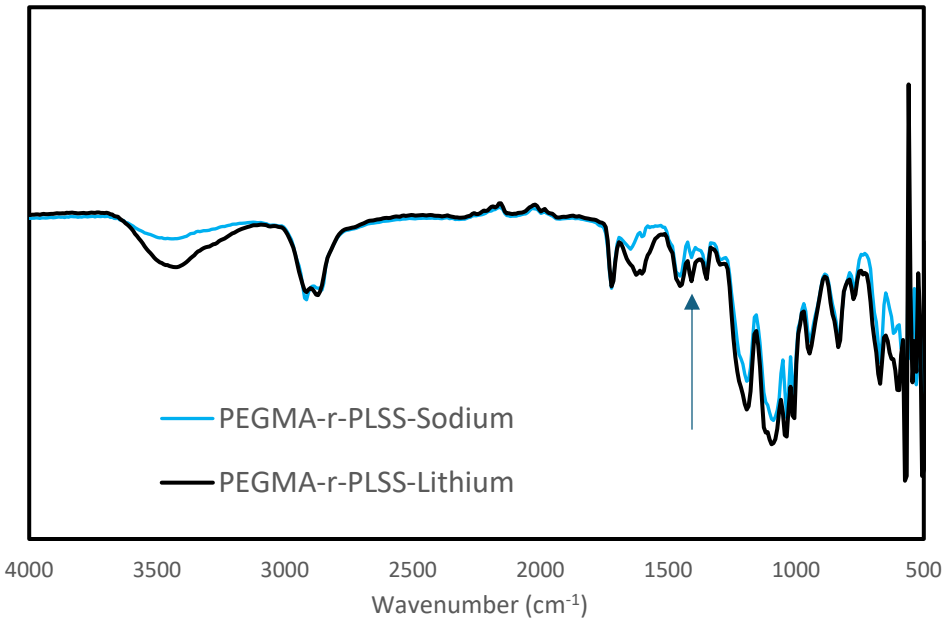

Figure 3.3 FTIR analysis and verification of ion exchange of PEGMA-r-PLSS-65 indicating the unique Li+ peak

3.4.2. Thermal Properties

Table 3.2 summarizes the analysis of the copolymer's thermal properties. The DSC data was analyzed to find the T_g by the midpoint method. Additionally, the T_g was first estimated using the Flory-Fox equation. From the literature, the T_g of PSS in the sodium form was found to be 228°C.[55] The PSS in the samples in this study are in the lithium form, so the T_g can be expected to vary. The T_g of PEGMA was previously found to be -62°C in literature.[56] The Flory-Fox equation is given in Equation 3.2, which shows the relationship between the weight percent and T_g.

$$\frac{1}{T_g} = \frac{w_1}{T_{g1}} + \frac{w_2}{T_{g2}} \quad (Flory - Fox\ equation)\ (Equation\ 3.2)$$

where w_x is the weight percent of polymer in the copolymer, and T_{gx} is the glass transition temperature of the individual polymer.

DSC curves (Figure 3.4) show a clear T_g for each RCP, varying with the different weight percentages of PEGMA/PLSS. Higher percentages of PEGMA have a low T_g close to that of pure PEGMA with the lowest PLSS copolymer (PEGMA-*r*-PLSS-12) composition having a lower T_g of -50 °C. All copolymers had T_g below room temperature, with the highest content of PLSS (PEGMA-*r*-PLSS-75) resulting in a T_g of 10°C. It is also important to note that there is no T_m peak in the DSC curve, meaning that the copolymer is amorphous by nature. Both PEGMA and PLSS have bulky side groups, which makes them unable to form ordered crystalline structures. The experimental results were compared to the theoretical results from the Flory-Fox equation in Table 3.2.

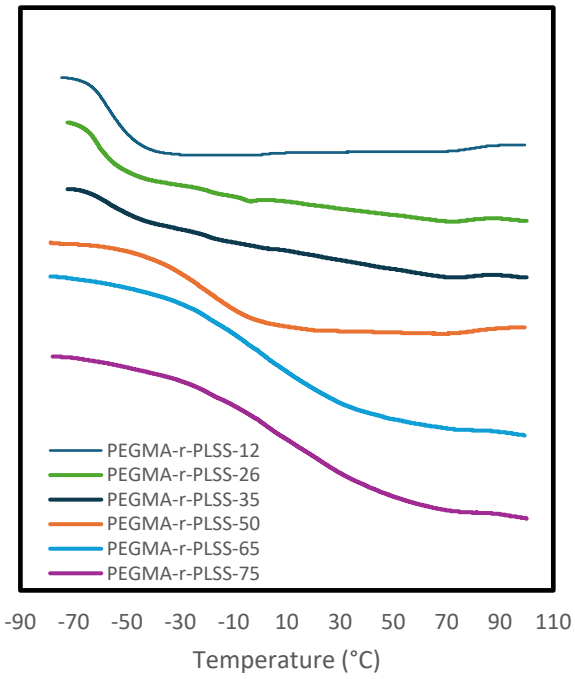

Figure 3.4 DSC curves of different PEGMA-r-PLSS compositions (Exo up)

At room temperature, all polymer samples will be above their T_g, i.e., the polymer will be in a rubbery, more flexible state. Above the T_g, polymer chains have enough thermal energy to

overcome the intermolecular forces that hold them in a fixed, glassy arrangement. As a result, the polymer becomes more flexible, allowing for molecular mobility, increased chain movement, and softer mechanical properties. Flexibility is highly desired for battery applications since it creates more free volume in the polymer electrolyte, enabling Li^+ ions to move more easily throughout the polymer chains and allowing for higher conductivity.[57] Flexible electrolytes can conform better to electrode surfaces, ensuring intimate contact and reducing interfacial resistance, which is crucial for efficient charge/discharge processes.[58] They are also less prone to mechanical failure, such as cracking which can lead to short circuits or battery failure. The ability to have flexible polymer electrolytes allows for easier processing into thin films or other desired shapes. Flexibility of the electrolyte must be balanced with the goal of excellent mechanical properties to prevent dendrite formation, as discussed earlier.

The thermal degradation behavior of the polymers was analyzed by TGA. An example TGA curve can be seen in Figure 3.5. The degradation temperatures (T_d) were taken to be when the copolymer sample reaches approximately 95% of its original mass and are given in Table 3.2. From the TGA curve, it is first seen that around 300°C significant degradation begins, breaking the polymer's main chain or side chains. After the TGA testing, it was noted that some porous carbon was formed. This could have potential for other applications such as H_2 storage for example.[59]

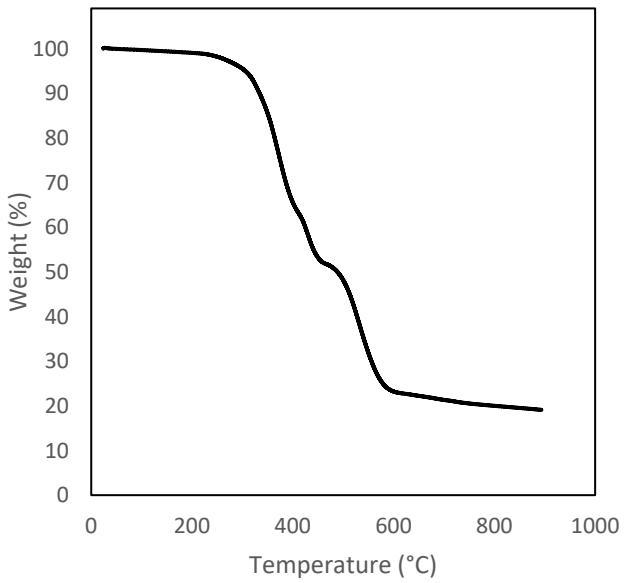

Figure 3.5 TGA curve of PLSS-r-PEGMA-50

A high T_d (i.e., >250°C for LMBs) is important for many reasons, including safety, performance, durability, and longevity.[60] High T_d of the polyelectrolyte indicates that the material will have better electrochemical stability, meaning that the polymer electrolyte can sustain higher voltages without decomposing, which is essential for high-energy-density batteries.[61] Batteries undergo repeated charge and discharge cycles, which can generate a large amount of heat. This could lead to thermal runaway, a dangerous condition where the battery generates heat uncontrollably, potentially leading to fires or explosions. Polymer electrolytes with a high thermal degradation temperature will help mitigate this risk by maintaining stability at elevated temperatures.[62] The results show that the polymers are thermally stable, with degradation temperatures around 300°C, indicating that the polymer electrolyte will be thermally stable in the battery's operating range.

Table 3.2 Summary of thermal properties of PEGMA-r-PLSS copolymers.

Copolymers	**Measured T_g from DSC (°C)**	**Theoretical T_g from Flory-Fox (°C)**	**T_d (°C)**
PEGMA-*r*-PLSS-12	-50	-53	250
PEGMA-*r*-PLSS-26	-50	-43	270
PEGMA-*r*-PLSS-35	-40	-35	280
PEGMA-*r*-PLSS-50	-25	-16	300
PEGMA-*r*-PLSS-65	0	10	300
PEGMA-*r*-PLSS-75	10	40	280

3.4.3. Film formation and Mechanical properties

Polymer processing to produce thin films can be challenging, due to issues like limited solubility or cracking. Here, the method of film formation is solution casting. A solvent must be determined that can effectively dissolve both parts of the copolymer while also being moderately volatile to produce uniform films. Numerous solvents were tried (e.g., methanol, DMSO, DIW), and DIW was the best candidate.

Films were originally cast to the desired thickness of ~50 μm from a 5 wt.% solution. While solution casting is not the most effective method for making uniform polymer films, and other techniques, such as doctor blade casting, are more effective at creating a uniform thickness, solution casting can be appropriate at small scale, particularly with limited material.[63] Still, from

solution casting, the thin films were prone to cracking or mechanical stress. Therefore, the solution concentration was increased to 10 wt% to ensure the films were durable enough for further testing. This resulted in a film thickness of ~100 µm, which is still appropriate for this application, while being much more mechanically durable.

The varying compositions of the copolymer significantly influenced the resulting film's mechanical and physical properties. Films with less PLSS exhibited a gel-like consistency, like PEGMA. In contrast, films with a higher molar percentage of PLSS became increasingly brittle and prone to cracking. This shift in properties can be attributed to the rigid and glassy nature of PLSS, which reduces the overall flexibility of the polymer matrix.[64] Thus, the balance between these two polymers plays a critical role in tailoring the mechanical behavior of the copolymer films.

While the copolymer films' mechanical properties were not quantitively tested, it was observed that the PEGMA-*r*-PLSS-50 exhibited the best film-forming properties. A photo of the film from this composition can be seen in Figure 3.6. Free-standing opaque, yellow films were produced. Film mechanical properties were not tested due to the hygroscopic nature of the polymers. Being exposed to the air allowed for the absorption of water, causing the films to change properties and lose the rigid properties that are required to stop dendrite formation. In an actual battery, no water would be exposed to the electrolyte; therefore, the mechanical properties tested would not be comparable if exposed to moisture in the air. Further research may involve the testing of the mechanical properties in an inert atmosphere to imitate battery conditions.

Figure 3.6 Polymer film from PEGMA-r-PLSS-50

3.4.4. Electrochemical Properties

The ionic conductivity of the PEGMA-*r*-PLSS copolymers across a temperature sweep can be seen in Figure 3.7. Conductivity increases with temperature according to the Arrhenius equation.[65] The highest conductivity is observed for PEGMA-*r*-PLSS-12, which has a high conductivity of 2.2 x 10^{-5} S cm^{-1} at room temperature and 2.3 x 10^{-4} S cm^{-1} at 70 °C. These values are considered satisfactory by current industry standards; they are similar to other works based on PEGMA and PLSS copolymers such as the work of Kwon et al.[6,53] When compared to similar polymer such as the work of Kwon et al. with a longer EO chains on PEGMA, the ionic conductivity values from this study obtained higher values, which aligns with research since the shorter PEGMA chains will allow for more flexibility since they will not be able to form semicrystalline domains which is an issue for longer EO chains.[53] When compared to the work of Wang et al. the ionic conductivity values are higher in this study are higher which is expected since the Li+ ion is smaller in size compared to the Na+ ion.[32] It should be noted that these PEGMA-r-PLSS polymers have not been synthesised in Li+ form. A comparison of values obtained can be seen below in Table 3.3.

Table 3.3 PEGMA-r-PLSS compared to similar polymers

Polymer electrolyte	σ (RT)	σ (70 °C)	Ref.
PEGMA-r-PLSS-12	$2.2\ x\ 10^{-5}$	$2.3\ x\ 10^{-4}$	This work
PEGMA-r-PLSS-50	$1.59\ x\ 10^{-6}$	$1.4\ x\ 10^{-4}$	This work
PEGMA-r-PSS (Na+ form)	$1.1\ x\ 10^{-7}$	$4.0\ x\ 10^{-6}$	[32]
PEGMA-r-PLSS (longer EO chain in PEGMA)	$6.0\ x\ 10^{-6}$	$5.\ 0\ x\ 10^{-5}$	[53]
PLSS/PEO blend	$1.1\ x\ 10^{-8}$	$1.0\ x\ 10^{-6}$	[37]
Commercial polymer (NEI Nanomyte H-polymer)	$5.0\ x\ 10^{-5}$	$8.0\ x\ 10^{-4}$	[66]

The PEGMA units contribute to high ionic mobility due to their flexible EO chains. These chains create a microenvironment that enhances ion dissociation and reduces ion pairing, facilitating more effortless movement of ions. The reduced crystallinity from the increased PEGMA enhances segmental motion, further improving ion transport. Some other trends are also visible from the conductivity data. First, the general trend with increasing PLSS content is that the conductivity generally decreases. However, there are exceptions to this trend, such as for PEGMA-*r*-PLSS-50, the conductivity is much higher, especially at higher temperatures, than even many other samples with lower PLSS content. This may be because the PEGMA-*r*-PLSS-50 sample is at the optimal [EO]/[Li^+] ratio of around 9:1 which directly shows the increase in conductivity.[37] At around 60 °C, the PEGMA-*r*-PLSS-50 samples reach over 10^{-4} S cm^{-1}, making them competitive with the PEGMA-*r*-PLSS-12 samples.

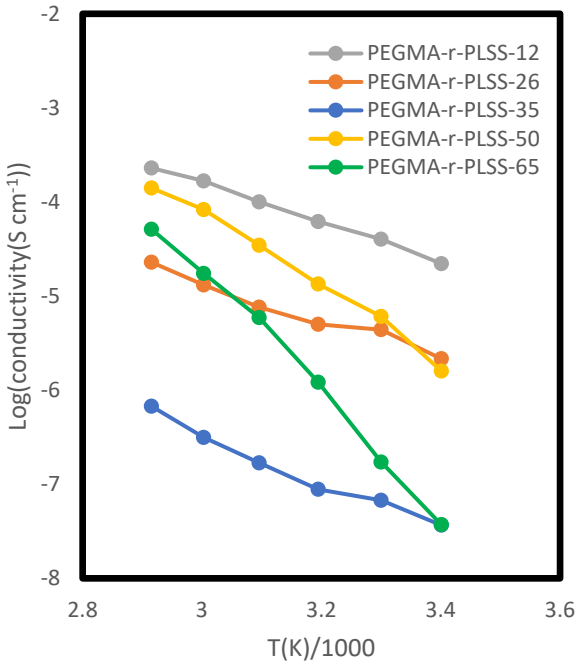

Figure 3.7 PEGMA-r-PLSS conductivities from room temperature to 70 °C

The increase of PLSS content can cause a decrease in conductivity for multiple reasons. Much of this goes back to the [EO/Li^+] ratio, which is directly related to the PEGMA:PLSS ratio in each RCP. Having too high of a percentage of PLSS (i.e., low [EO]/[Li^+] ratios) means there are not enough coordination sites for the lithium ions, causing a decrease in conductivity, as seen for PEGMA-*r*-PLSS-65.[67] Alternatively, initially when going higher than the optimal [EO]/[Li^+] ratio

the conductivity also drops as seen in PEGMA-*r*-PLSS-35. However, even higher percentages of PEGMA (i.e., higher [EO]/[Li^+] ratios) ultimately show an increase in conductivity overall up to the highest overall, PEGMA-*r*-PLSS-12. The effect of temperature is also much more noticeable in the higher percentage of PLSS samples. For example, PEGMA-*r*-PLSS-65 starts at a lower conductivity at room temperature, yet it climbs multiple magnitudes from 10^{-8} S cm^{-1} to over 10^{-5} S cm^{-1}. A similar effect is seen for PEGMA-*r*-PLSS-50 and for the lower molar percentage PLSS samples, only about an increase of one order of magnitude. Higher PLSS content may increase the rigidity of the polymer matrix, hindering ion mobility. According to the Arrhenius equation (Equation 3.3), the conductivity of a material (σ) depends on the activation energy (E_a) and temperature (T).[68] Based on the Arrhenius equation, the activation energy (E_a) increases as the mol% of PLSS increases, indicating that higher PLSS content creates greater resistance to ion transport.[69]

$$\sigma = \sigma_0 \exp\left(\frac{-E_a}{k_B T}\right) \ (Arrhenius\ equation) \ (Equation\ 3.3)$$

where σ_0 is the pre-exponential factor, k_B is the Boltzmann constant, E_a is the activation energy. and T is the temperature.

The two samples with the highest PLSS content (PEGMA-*r*-PLSS-65 and PEGMA-*r*-PLSS-50) display different, yet similar, slopes in their Arrhenius plots. The higher slope for PEGMA-*r*-PLSS-65 suggests greater resistance to ion transport, consistent with the more rigid polymer matrix resulting from its higher PLSS content.[70] The lower slope for PEGMA-*r*-PLSS-50 implies a lower activation energy and improved ion mobility. This trend supports that increasing PLSS content stiffens the polymer matrix, creating higher activation energy barriers that reduce ion mobility.[70]

Another way to observe the conductivity data is to plot it against reduced temperature, T_g/T, to view the conductivity without the contribution of polymer chain segmental motion.[71] This is plotted in Figure 3.8. Conductivity often follows the Arrhenius equation; however, deviations from Arrhenius behavior are common in glassy materials.[70] A reduced temperature plot helps highlight such deviations and may reveal the influence of dynamic processes such as ion hopping, ion mobility differences, ion aggregation, and charge carrier concentration.[71,72] This allows the influence of other factors on ion conductivity to be more clearly revealed. Figure 3.8 shows all compositions follow a similar trend of decreasing conductivity with increasing T_g/T, consistent

with the universal behavior of glassy or amorphous ionic conductors. The trend implies that the conductivity is strongly influenced by the material composition, with higher ratios of PLSS likely hindering ionic mobility, which could be caused by changes in free volume, segmental dynamics, or ion-solvent interactions that affect ion transport efficiency. If the plot of conductivity by T_g/T showed no differences from other factors, the conductivity data would fall under one line. Therefore, it is determined that other factors as stated above have a factor on the ionic conductivity of the samples. It can also be noted that the copolymers herein are highly hygroscopic, and thus, one concern regarding conductivity values is whether the materials are absorbing trace amounts of water in the atmosphere. This phenomenon could potentially lead to an overestimation of the measured conductivity values, particularly at high PEGMA content.

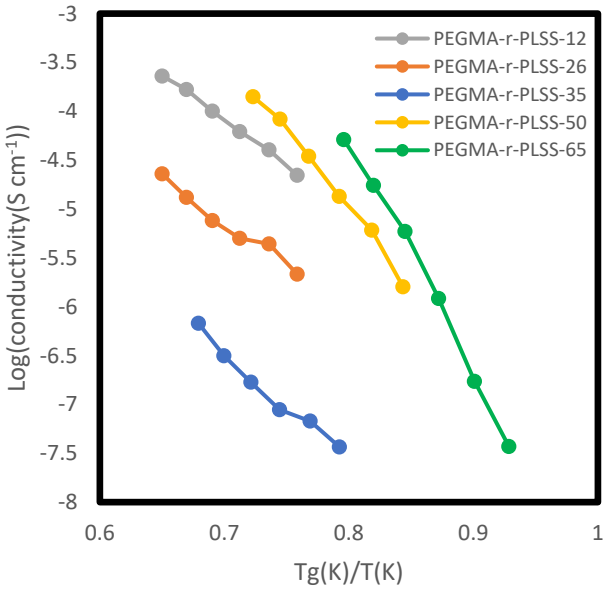

Figure 3.8 PEGMA-r-PLSS conductivities compared to Tg/T

Considering mechanical properties, PEGMA-*r*-PLSS-50 had quantitively the best mechanical properties for film formation, making thin, flexible films. Though PEGMA-*r*-PLSS-12 had the best conductivity, the film was observed to be more gel-like, not having a rigid structure. These properties made it difficult to obtain a free-standing polymer electrolyte, and in an actual LMB, this gel-like structure is likely unable to block the formation of dendrites.[73] When considering the trade-offs between Li-ion transport and SIPE mechanical properties, the best overall candidate is the sample with the optimal [EO]/[Li^+] ratio of 9:1, PEGMA-*r*-PLSS-50.

3.4.5. Conclusions

In this study, RCPs of PEGMA-*r*-PLSS were synthesized at six PLSS compositions ranging from 12 to 75 mol% PLSS and assessed for their potential for application as SIPEs in LMBs. PEGMA-*r*-PLSS-12 exhibited the highest conductivity, but the best candidate overall was PEGMA-*r*-PLSS-50, as it exhibited ion conductivity of the same order of magnitude while also forming films with good mechanical integrity.

Overall, the initial objectives for this project were satisfied with a range of different PEGMA-r-PLSS copolymers synthesized and characterized. The optimal EO:Li+ ratio was once again confirmed to be 9:1. Films were successfully made with RCPs exhibiting promising electrochemical properties. These findings show the versatility of the copolymer system, enabling optimization to meet specific application requirements. These copolymers hold significant promise for advancing energy storage technologies, offering improved efficiency and reliability for next-generation battery systems.

4. PLVS blends for lithium metal batteries

4.1. Introduction

With the high demand for increasing the energy density of LMBs, many new polymers are being explored as SPEs for battery applications. Polyvinyl sulfonic acid (PVSA) is a synthetic polymer with sulfonic acid groups (-SO_3H) attached to its vinyl backbone, granting it high ionic conductivity and hydrophilicity. This unique combination of properties makes PVSA an attractive material for electrochemical applications, particularly in lithium metal batteries (LMBs), which are pivotal for next-generation energy storage systems.

PVSA is not a common polymer used for many applications except for hydrogels mainly due to its hydrophilic properties.[74,75] However, it also exhibits high proton conductivity, making it a possible candidate for polymer electrolytes. In the work of Okayasu *et al.*, PVSA was able to reach 10^{-5} S/cm^{-1} at room temperature, 10^{-4} S/cm^{-1} at 60ºC, and 10^{-3} S/cm^{-1} at 90ºC.[76] PVSA in lithium form has not been tested, making it interesting to explore. PVSA synthesis can also be done with water as a solvent, making it safe and cost-effective.[77] This is incredibly beneficial on a large scale since it will be cheaper and more environmentally friendly. PVSA was ion-exchanged to lithium form to form poly(lithium vinyl sulfonate) (PLVS). Incorporating PLVS with another polymer, such as PEGMA, was considered in a copolymer setting, yet PEGMA can be challenging to create copolymers with due to its large, bulky structure. Therefore, a blend of the two polymers was considered a starting point to observe the effect on the combined properties.

Considering the solubility of PLVS, the best option to blend these two polymers for casting was DIW, which partially dissolved the PEGMA homopolymer due to the methacrylate section on the PEGMA.[78] Since the PEGMA-*r*-PLSS copolymers made are water soluble, it was chosen to synthesize the PLVS separately and blend it with the lowest composition PLSS, highest conductivity RCP (PEGMA-*r*-PLSS-12). The [EO]/[Li^+] ratio is an important factor since it was confirmed that the most optimal ratio was found to be 9:1, in agreement with literature.[37] Since the PEGMA-*r*-PLSS-12 was used, this sample did not contain much PLSS with a high EO ratio of 66:1. This could be doped with PLVS in a blend to reach the optimal [EO]/[Li^+] ratio of 9:1. However changing polymer structure may effect the optimal EO:Li+ ratio therefore 20:1 was also tested to observe the overall trend. Having a lower amount of PLSS will lower the mechanical

properties of the electrolyte but it could cause a significant increase in conductivity. As stated before, the electrochemical properties should be optimized first; then mechanical properties can be tailored to stop dendrite formation. PLVS could prove to be a potential candidate for shifting the research of polymer electrolytes in a new direction. The structure of PLVS can be seen below in Figure 4.1.

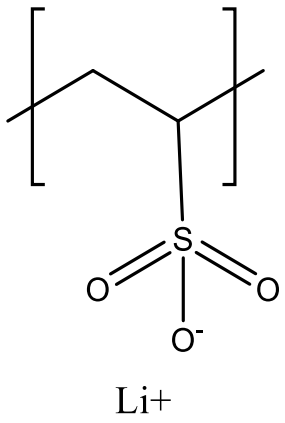

Figure 4.1 Structure of PLVS

4.2. Experimental

4.2.1. Materials.

Vinyl sulfonic acid sodium salt solution (VSA) 25 wt.% in H_2O purchased from Sigma Aldrich was purified with an inhibitor-remover column to remove the (MEHQ) inhibitor. Ammonium Persulfate (APS) was used as an initiator purchased from Sigma Aldrich. Deuterium oxide (D_2O, ≥99.9%) was purchased from Cambridge Isotope Laboratories. Lithium hydroxide monohydrate (LiOH, 99.0%) was purchased from Sigma Aldrich.

4.2.2. Synthesis of PVSA.

The synthesis of PVSA followed a modified procedure of Okayasu *et al.* using free radical polymerization to achieve high MW PVSA.[76] The polymerization process begins by pre-heating a silicon oil bath to 60°C. Meanwhile, prepare for a freeze-pump-thaw cycle by setting up a vacuum trap with liquid nitrogen, arranging a nitrogen gas flow, and preparing a needle stopper and zip tie for a Schlenk flask. In the Schlenk reaction, add VSA with 0.1wt% APS. Since the VSA is in water already, no additional solvent is needed for the reaction. The flask is then connected to the freeze-pump system, where three freeze-pump-thaw cycles are performed. The flask is placed in the silicon bath for 24 hours. Unreacted monomer and lower MW polymers were removed by

dialysis with DIW using a Slide-A-Lyzer G2 dialysis cassette with a 3500 MW cut-off with 70 ml sample size. The reaction product was first quenched with liquid nitrogen. The mixture was then thawed and added to the dialysis cassette, and the remaining space was filled with DIW. The cassette was immersed in a 4 L beaker filled with DIW while the dialysate was changed with DIW every 2 to 4 h for roughly 10 hours total. The solution was removed from the cassette tape, and the excess DIW was removed using a rotary evaporator. The remaining concentrated solution was then vacuum-dried at 80 °C for 24 h (yield: 48%).

4.2.3. Ion Exchange Metathesis.

The PVSA synthesized must be ion exchanged from the sodium ion to lithium (PLVS) for further testing. This was done by first dissolving the PVSA in DIW, using ~10 ml for every 0.25 grams of PVSA. Then LiOH was added in a 10:1 molar ratio LiOH:PVSA to ensure that there were enough lithium ions to be exchanged. The solution was mixed for 24 hours at 60 °C. The solution started out clear at the beginning of the reaction, changed color to a light green color temporarily, then turned to a yellow colour near the end of the reaction. The polymer sample was removed by dialysis with DIW using a Slide-A-Lyzer G2 dialysis cassette with 2000 MW cutoff with 15 ml sample size. The solution was removed from the cassette tape and the excess DIW was removed using a rotary evaporator. The remaining concentrated solution was then vacuum-dried at 80 °C for 24 h (yield: ~50-60%).

4.2.4. Polymer casting

PEGMA-*r*-PLSS-12 samples were blended with PLVS at two different [EO]/[Li^+] ratios of 20:1 and 9:1. Polymer samples were dissolved in DIW (5 or 10 wt% polymer, depending on solubility) and stirred overnight to ensure complete dissolution. The solution was then cast onto a Teflon sheet in a petri dish, covered with a glass funnel, and left ~2 days while the solvent evaporated. The funnel was removed, and the casts dried in ambient conditions for another 24 h. The casts were then placed in the vacuum oven, dried at 80 °C without vacuum for ~3 h, then dried under vacuum for 24 h. After drying, polymer films were removed from the Teflon as free-standing films.

4.3. Characterization.

4.3.1. Proton Nuclear Magnetic Resonance Spectroscopy (^{1}H NMR).

^{1}H NMR spectra were recorded on a Bruker Avance III 500 MHz with TOPSPIN software. D_2O (~1 mL) was used to dissolve ~5 mg of copolymer sample. Chemical structures were determined from the ^{1}H NMR spectra, with all peaks assigned and quantitatively understood.

4.3.2. Fourier-Transform Infrared Spectroscopy (FTIR).

FTIR spectra were recorded using Agilent Cary 630 FTIR Spectrometer. FTIR was used to confirm the success of the ion exchange between the sodium and lithium ions.

4.3.3. Gel permeation chromatography (GPC)

GPC was recorded using Thermal Scientific Ultimate 3000 HPLC to determine the MW of the polymer samples. The device was calibrated using polystyrene standard samples to ensure accurate MW. Due to their ionic properties, samples were run in DMF columns with 0.05 M LiBr at 35 °C with a flow rate of 1 mL/min.

4.3.4. Thermal properties.

Thermal gravimetric analysis (TGA; TA Instruments, Q550) measured the copolymers' thermal degradation using a temperature ramp to 800 °C at a heating rate of 10°C min^{-1} under an N_2 environment. The polymer's thermal behavior was observed by differential scanning calorimetry (DSC; TA Instruments, Q2000) over a temperature range of -90 to 180 °C at a heating/cooling rate of 10°C min^{-1} under an N_2 environment using a heat/cool/heat method. The glass transition temperature was analyzed by midpoint method using TA instruments Trios analysis software.

4.3.5. Electrochemical properties

The ionic conductivities of polymer films were measured with electrochemical impedance spectroscopy (EIS) over a frequency range of $10-10^6$ Hz at 10 mV. Six different points were taken at room temperature: 30, 40, 50, 60, and 70 °C. The conductivities of the polymer films were measured in a split cell (MTI split cell for R&D battery 15mm I.D.) with a two-electrode setup, where an alternating current was applied across the two electrodes, and the actual impedance or resistance, R, was determined from the measured voltage and current. The resistance was determined from the high x-intercept of the semicircle regression of the Nyquist plot using the EC-

lab software. An example Nyquist plot can be seen in Appendix A.4. Conductivity was calculated using Equation 4.1,

$$\sigma = \frac{L}{AR} \qquad Equation\ 4.1$$

where L is the distance between electrodes, A is the cross-sectional area of the polymer film, and R is the resistance.

4.4. Results and discussions

4.4.1. Chemical properties

^{1}H NMR spectroscopy was used to identify the structure of PLVS, given in Figure 4.2. Peak A (~4.0 ppm) corresponds to the methine (-CH-) protons directly bonded to the sulfonate group (-SO_3^-). The deshielding effect of the sulfonate group shifts these protons to a higher chemical shift. Peak B corresponds to 2 protons at 1.5–2.5 ppm, arising from the methylene (-CH_2-) protons in the polymer backbone adjacent to the methine group. The broader and overlapping nature of these peaks suggests some flexibility or structural variation in the polymer chain. The sulfonate functional group attached to the polymer backbone has a strong electron-withdrawing effect, influencing the chemical environment of nearby protons (A and B). The relatively broad peaks for B indicate the polymeric nature of the material, where conformational differences along the chain create slight variations in the local magnetic environment.

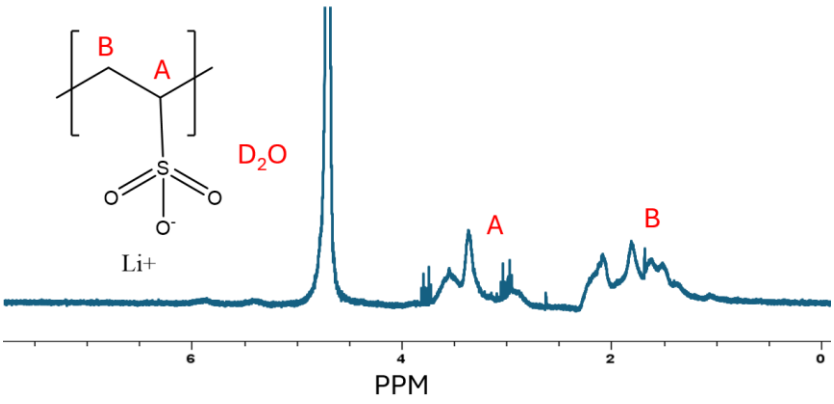

Figure 4.2 PLVS NMR

FTIR was used to confirm the success of the ion exchange (Figure 4.3). The unique peaks from the lithium cation can be identified from the peaks at approximately 1500 cm^{-1}. The peak at approximately 800 cm^{-1} is also attributed to lithium. These peaks were assigned based on the work

of Park et al. for the analysis of PSS to PLSS.[37] Although PVSA has a different structure from PLSS since it does not contain the benzene ring, the same peaks appear, ensuring the ion exchange was successful. However, the peaks are much less prominent than those of PLSS, meaning that the exchange may only be partial and only exchange a fraction of the PVSA to PLVS. This would have to be further tested to ensure the ion exchange is complete since FTIR will only qualitatively determine the success of the ion exchange in this case.

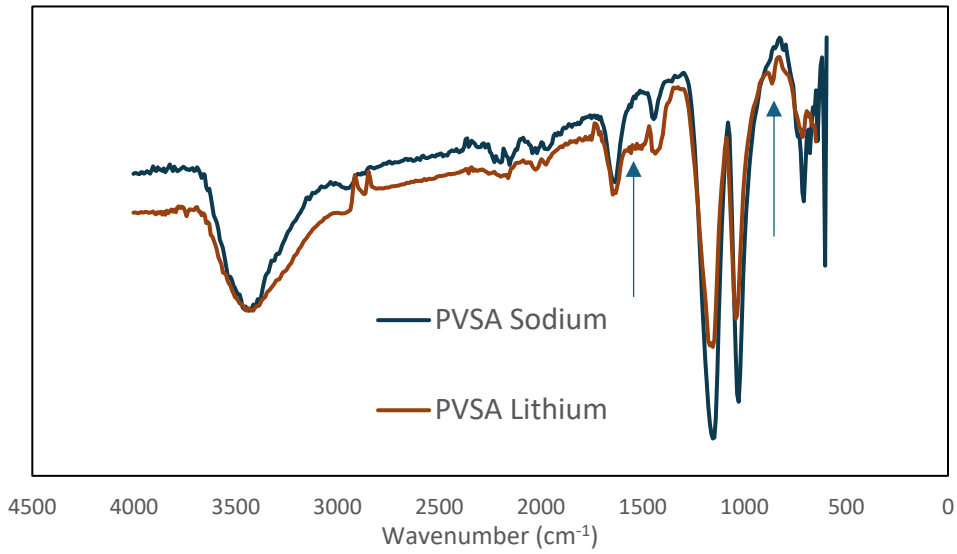

Figure 4.3 PVSA to PLVS FTIR to confirm ion exchange from sodium to lithium-ion form

The number average MW of PLVS was found by GPC (Figure 4.4) to be ~10 kDa with a PDI of 1.33. This is a sufficient polymer chain length for the application, with a moderately narrow MW distribution.

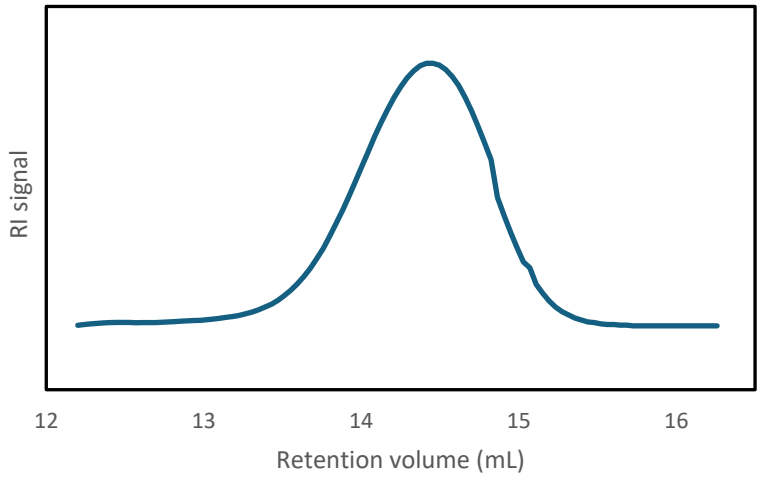

Figure 4.4 GPC Curve of PLVS

4.4.2. Thermal properties

TGA was used to analyze the thermal stability of the PLVS and determine the degradation temperature. The degradation temperatures (T_d) were taken to be when the copolymer sample reached approximately 95% of its original mass. The TGA curve can be seen below in Figure 4.5a. The degradation temperature is found to be 275 °C, which means the polymer is thermally stable for LMBs. From the TGA curve, after 350 °C, the polymer begins to degrade rapidly, causing rapid mass loss. The DSC thermograph for PLVS shows a T_g of around -55 °C (Figure 4.5b). This low glass transition temperature benefits LMBs by increasing the flexibility of the lithium ions' movement and increasing conductivity. Additionally, the increased flexibility at a molecular level helps maintain electrolyte stability and prevents the formation of rigid structures that could hinder ion transport, especially at lower operating temperatures. Consequently, this property contributes to better overall battery performance, such as higher power density, faster charging rates, and improved functionality in diverse environmental conditions.

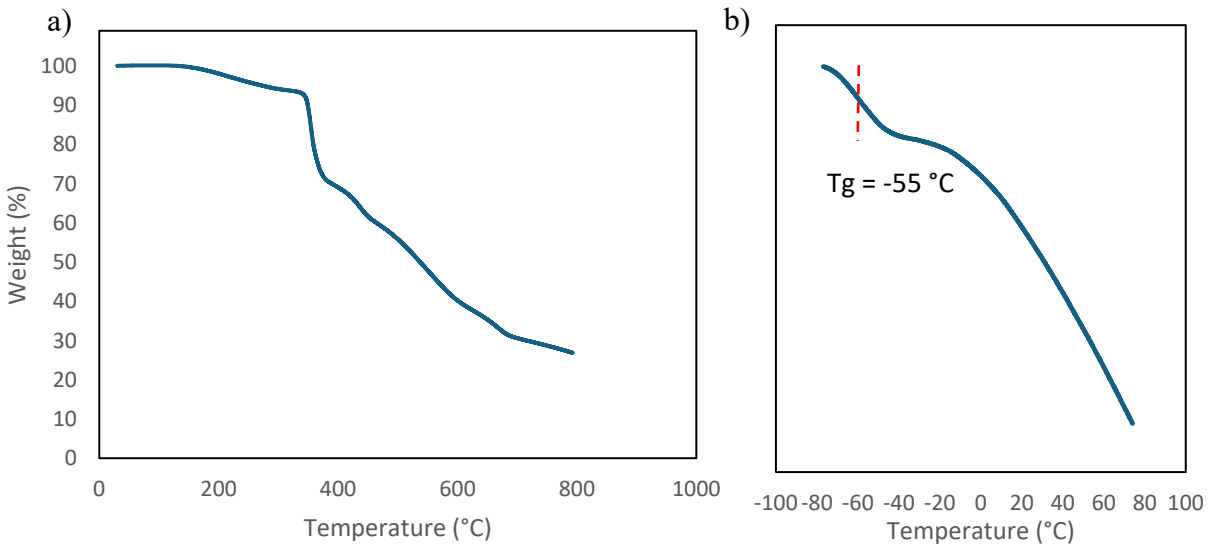

Figure 4.5 Thermal characterization of PLVS: a) TGA and b) DSC (Exo up).

4.4.3. Electrochemical properties

The two RCP/PLVS blends were run and compared to the ionic conductivity of PEGMA-*r*-PLSS-12. Despite its low T_g, PLVS was not found to increase conductivity; instead, it decreased conductivity. The added PLVS dropped the conductivity by over 2 orders of magnitudes with the 20:1 doped sample and almost 3 orders of magnitudes for the 9:1. At the higher temperatures, the conductivity increased by about an order of magnitude but overall was significantly lower than the PEGMA-*r*-PLSS-12. The conductivities for the doped PLVS/PEGMA-r-PLSS-12 blends can be seen in Figure 4.6.

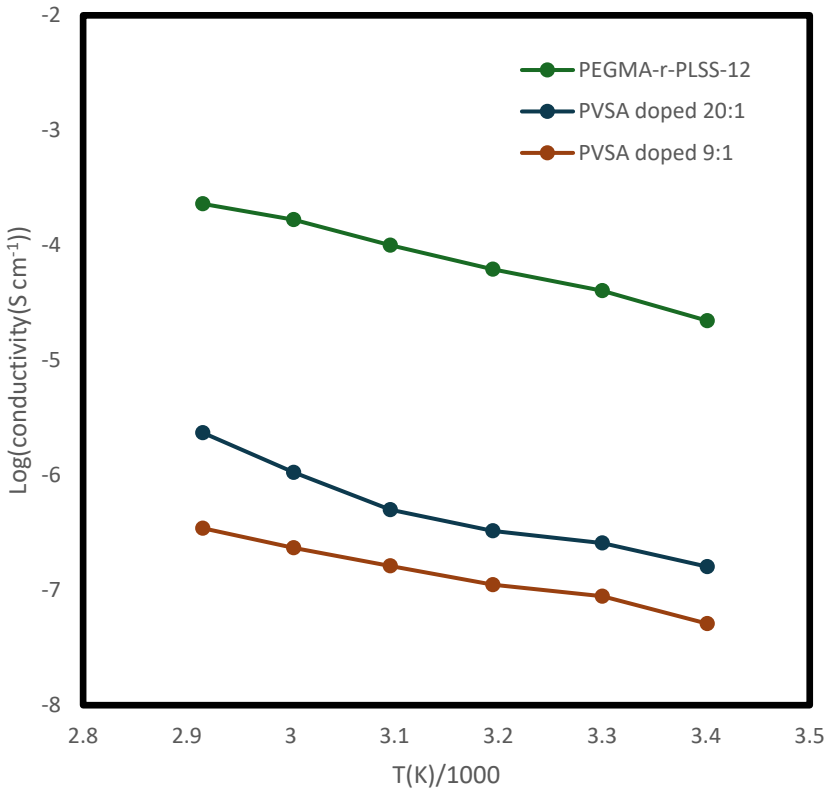

Figure 4.6 The conductivity of PLVS/PSS-r-PLSS blends

While the blend's conductivity is lower, PLVS may still have potential. These are physical mixtures of two polymers. The different polymers in the blend often phase-separate due to incompatibility, creating distinct domains with varying properties.[79] This could create areas in the electrolyte with concentrated areas of PLVS and other areas higher in PEGMA-*r*-PLSS-12, increasing polarization since the lithium ions would move toward areas with higher PLVS concentrations. Ion mobility can be hindered due to limited continuity in the conductive pathways.[80] In PEGMA-*r*-PLSS copolymers, the lithium ions can interact with PLSS distributed along the chain. This random distribution ensures more continuous solvation and transport routes for ions.

In blends, the interfaces between different polymer domains can act as barriers to ion movement, further reducing conductivity. The interfaces between different polymer domains can act as barriers to ion movement, further reducing conductivity. To overcome this issue, compatibilizers can be introduced to improve interfacial adhesion and promote a more homogeneous microstructure. These additives reduce phase separation by lowering interfacial energy and enhancing molecular

interactions between polymers.[81] By creating a more interconnected and stable morphology, compatibilizers facilitate smoother ion transport pathways, thereby improving both mechanical integrity and electrochemical performance.

The effect of blending PLVS with PEGMA-PLSS was the focus of this section; therefore, the conductivity of neat PLVS was not tested. The conductivity was high for PVSA in H^+ form, but when ions exchanged to Li+ to form PLVS, this may have had a negative impact on ionic conductivity due to the increased ion size of the Li^+ ion.[82] Further testing should include testing the conductivity of PLVS.

Other approaches could involve synthesizing a copolymer with PLVS. There is a considerable lack of methods for copolymerizing PVSA and PLVS with other monomers, such as free radical polymerization. Copolymers using free radical polymerization were found challenging to synthesize due to the strong electron-withdrawing property and the steric bulkiness of the SO_3^- group.[76] This makes it difficult to synthesize desired molar ratios and high PVSA content. Notably, many studies have instead focused on crosslinking PVSA to create copolymers, especially in applying hydrogels.[74]

4.4.4. Conclusions

Based on initial objectives, PLVS was successfully synthesized and characterized; however, it was not found to increase ionic conductivity when blended with PEGMA-*r*-PLSS-12. Investigating the possibility of adding a compatibilizer to improve blends may be a potential option, but further research could focus on synthesizing a random copolymer with PLVS and PEGMA to overcome the limitations of simply blending the two components. This approach would achieve a more uniform distribution of properties, incorporating the desired functional groups into a single polymer backbone. Future research should investigate whether PLVS can effectively be integrated into random LMB electrolyte copolymers.

5. PEGMA-*b*-PLSS block copolymers for lithium metal batteries

5.1. Introduction

Block copolymers (BCPs) offer significant advantages over random copolymers for LMBs. Due to their unique structure, they consist of distinct polymer blocks covalently bonded together, which promotes better phase separation. This phase separation enables the design of polymer electrolytes with separate ion-conducting and mechanically robust domains, addressing the trade-off between ionic conductivity and mechanical stability.[44] The well-defined nanostructure of BCPs enhances lithium-ion transport while maintaining the dimensional stability needed to suppress dendrite growth on lithium metal anodes.[44,83] These properties make block copolymer-based electrolytes highly promising for advancing the safety and performance of next-generation LMBs.

Herein, synthesis of a BCP analog of the RCP from Ch.3 was explored. In addition, the BCP could also be functionalized with stronger electron-withdrawing groups to reach the highest possible ion conductivity. The first step was to make PS macro-chain transfer agent (CTA). 4-Cyano-4-(phenylcarbonothioylthio)pentanoic acid was chosen due to its compatibility with the methacrylate backbone, which the PEGMA contained, as well as PS. After the PS-CTA is synthesized, the PEGMA group is added as the second block. Last, the PS is functionalized with an electron-withdrawing groups such as lithium sulfonate or a more delocalized anion (pictured), to be added through a series of steps (Figure 5.1).

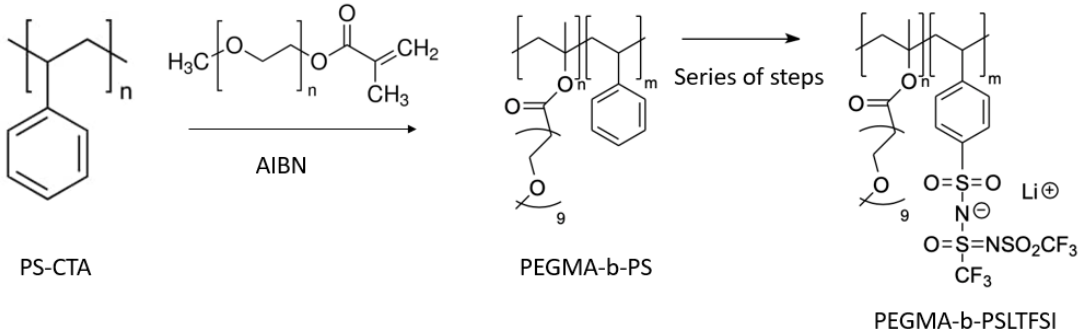

Figure 5.1 Synthesis of PEGMA-b-PS with further steps

5.2. Experimental

5.2.1. Materials.

Deuterated chloroform ($CDCl_3$, ≥99.9%) was purchased from Cambridge Isotope Laboratories. All other chemicals were purchased from Sigma Aldrich and used as received unless otherwise noted. Styrene was purchased from Sigma Aldrich and purified with an inhibitor-remover column to remove the tert-butylcatechol inhibitor. Poly(ethylene glycol) methyl ether methacrylate (PEGMA) with an average Mn of 500 was purified with an inhibitor-remover column to remove the (MEHQ) inhibitor. The initiator 2,2′-azobis- (isobutyronitrile) (AIBN) was purchased from Sigma Aldrich and was recrystallized twice from methanol before use. N,N- dimethylformamide (DMF, ACS Reagent, ≥99.8%) was purchased from Fisher Scientific. The chain transfer agent 4-Cyano-4-(phenylcarbonothioylthio)pentanoic acid was purchased from Sigma Aldrich.

5.2.2. Synthesis of PS-CTA.

The polymerization process begins by pre-heating a silicon oil bath to 60°C. Combine the CTA and styrene in the Schlenk flask. The different ratios tested can be shown later in Figure 5.3. Before the reaction, three freeze−pump−thaw cycles were applied to the reactant solution with liquid nitrogen under vacuum to remove oxygen and moisture from the reaction chamber. The flask is placed in the silicon bath for 20 hours. Once the polymerization is complete, the gas is shut off, and the product is poured into a large amount of methanol to wash out any unreacted monomer. The final product was removed using vacuum filtration and rewashed in methanol at least 2 more times. The final product was dried in the vacuum oven at 60° C for 24 hours.

5.2.3. Synthesis of PS-*b*-PEGMA.

The synthesis procedure was based on the work of Porcarelli et al.[56] The polymerization process begins by pre-heating a silicon oil bath to 70°C. Meanwhile, prepare for a freeze-pump-thaw cycle by setting up a vacuum trap with liquid nitrogen, arranging a nitrogen gas flow, and preparing a needle stopper and zip tie for a Schlenk flask. In the Schlenk reaction flask, combine PEGMA, PS-CTA, AIBN and DMF. Many different ratios were tried, and a summary can be seen in Table 5.1. The flask was then connected to the freeze-pump system, where three freeze-pump-thaw cycles are performed. Each cycle involves freezing the solution, vacuuming for 3 minutes, and thawing in water while turning on the nitrogen gas. The flask is placed in the silicon bath for 8 hours. Once the polymerization is complete, the gas is shut off, and the product was poured into a large amount

of methanol to wash out any unreacted monomer. The final product was removed using vacuum filtration and rewashed in methanol at least 2 more times. The final product was dried in the vacuum oven at 60° C for 24 hours.

5.3. Characterization of PS-CTA/PS-PEGMA.

5.3.1. Proton Nuclear Magnetic Resonance Spectroscopy (^{1}H NMR).

^{1}H NMR spectra were recorded on a Bruker Avance III 500 MHz with TOPSPIN software. Deuterated chloroform ($CDCl_3$) (~1 mL) was used to dissolve ~5 mg of copolymer sample. Chemical structures were determined from the ^{1}H NMR spectra, with all peaks assigned and quantitatively understood. The NMR spectra was also used to check the MW of the PS-CTA since the unique end groups from the CTA have unique peaks in the NMR spectra. This allowed for calculating the number of repeat units of PS which allowed for the determination of MW.

5.3.2. Gel permeation chromatography (GPC).

GPC was recorded using Thermal Scientific Ultimate 3000 HPLC to determine the MW of the polymer samples in THF columns at 35 °C with a flow rate of 1 mL/min. The device was calibrated using polystyrene standard samples to ensure accurate MW.

5.4. Results and Discussion.

PS-CTA was analyzed by ^{1}H NMR as seen in Figure 5.2. The unique hydrogen peaks from the CTA at 7.5-8 ppm allow for the characterization of the number average MW of the PS-CTA samples. This peak corresponds to the benzene ring of the CTA. The number of hydrogens can be compared to the PS peaks to get the overall MW. Three different ratios of PS monomer:CTA were tested in a range from 100:1 to 300:1, which showed a linear relationship between the different ratios, summarized in Figure 5.3. The desired MW was around 10 kDa to ensure that the second monomer could still be added sequentially rather than forming a blend of polymers. It also had adequate repeat units to be out of the oligomer range, where mechanical properties might suffer.

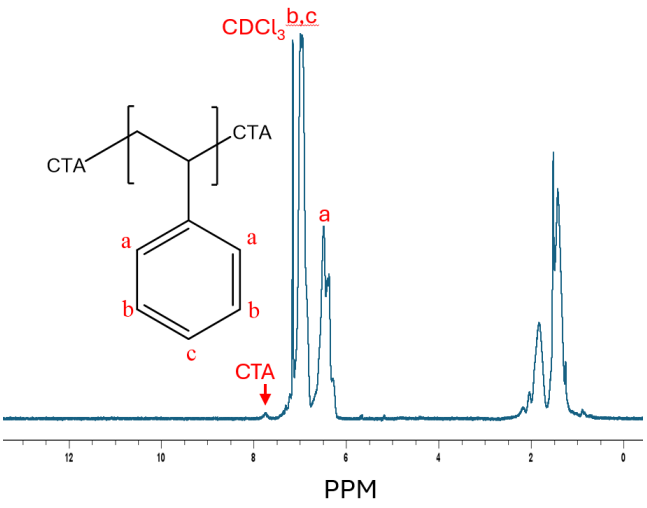

Figure 5.2 ^{1}H NMR of PS-CTA

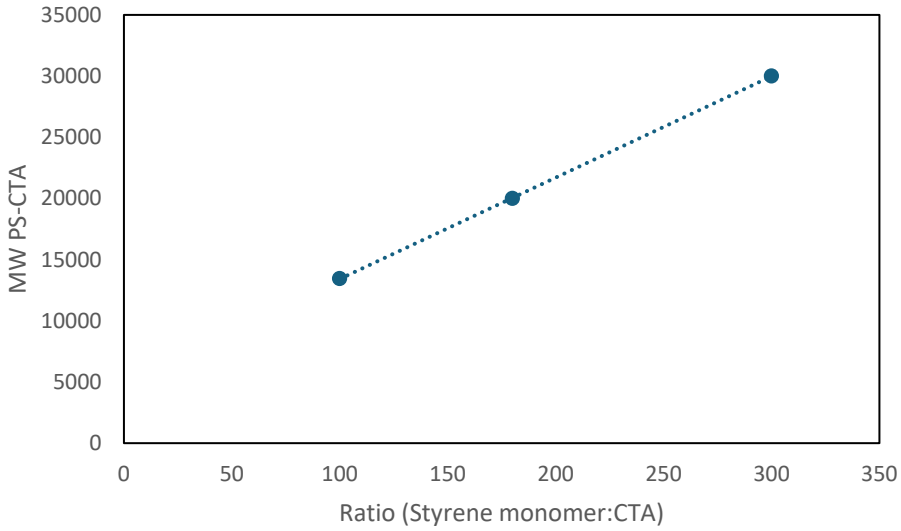

Figure 5.3 Relationship between monomer to CTA ratio and MW

PS-CTA was next chain extended with PEGMA monomer. One example of PS-*b*-PEGMA ^{1}H NMR spectra is given in Figure 5.4. Table 5.1 summarizes the synthesis attempts for PS-*b*-PEGMA based on differing MW PS-CTAs and their respective compositions as calculated from ^{1}H NMR.

Table 5.1 Summary of different synthesis procedures tried for PS-b-PEGMA

PS-CTA MW (g/mol)	Molar Ratio (PEGMA:PS-CTA:AIBN)	Mol% PEGMA	Yield, %
13,450	600:10:1	21.3%	53%
13,450	500:10:1	16.9%	46%
13,450	330:10:1	3.2%	10%
13,450	200:10:1	< 0.1%	46%
20,000	1000:10:1	< 0.1%	22%
30,000	3000:10:1	< 0.1%	15%
30,000	10000:10:1	< 0.1%	4%

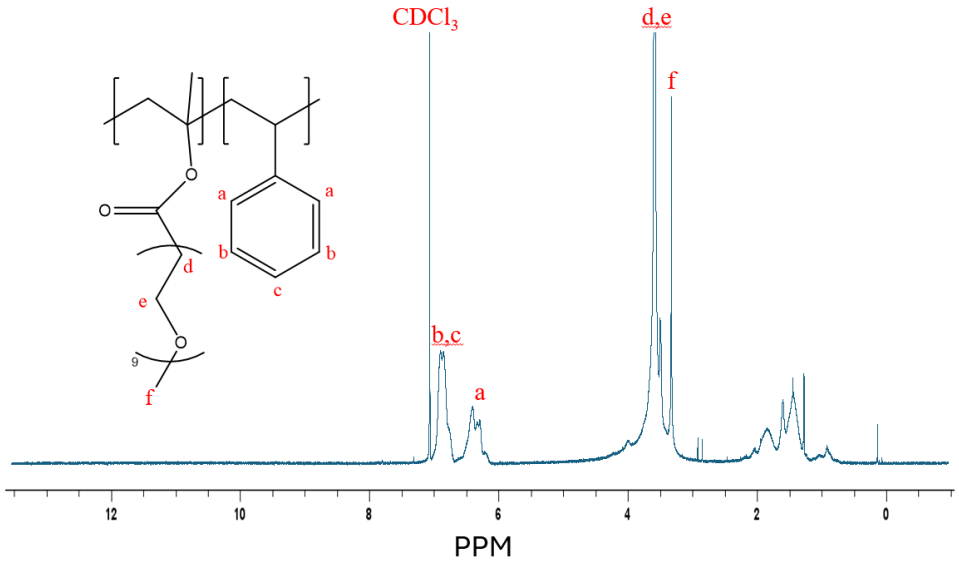

Figure 5.4 PS-b-PEGMA NMR

GPC (Figure 5.5) was used to confirm the MW of the PS-CTA 100:1 sample, as showed good agreement with ^{1}H NMR, confirming the MW was the same at ~13.5 kDa. The GPC was also used to analyze the PS-*b*-PEGMA samples. GPC curves of the BCPs (Figure 5.5) exhibited two distinct peaks indicative of two different polymer chains. This observation can be attributed to the formation of PEGMA homopolymer alongside the block copolymer or PS-CTA during the synthesis process. It was also noted that the PS-CTA elution peak did not change in elution volume compared to PS-*b*-PEGMA peak, which means very little, if any, PEGMA added. Likely, no BCP structure was achieved and rather a blend of homopolymers was made.

It has been noted in literature that PS-CTA may need to have MW ~5 kDa or less to successfully chain-extend with an acrylate- or methacrylate-based monomer and avoid homopolymer formation.[84] Moving forward, a PS-CTA could be synthesized at 5 kDa by utilizing a [monomer]/[CTA] ratio of <<100 (see Figure 5.3), which may enable PEGMA chain extension in the copolymerization step. Considering the high MM of the PEGMA monomer, even if the PS-CTA has low MW, if significant PEGMA is successfully added, the overall MW should be sufficient for adequate mechanical properties.

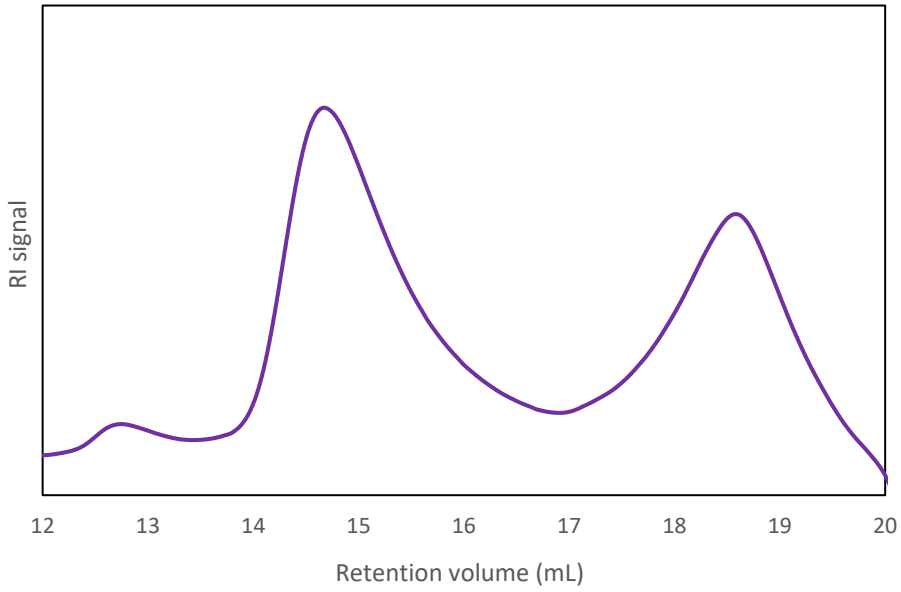

Figure 5.5 PS-b-PEGMA 500:10:1 with 9000 MW PS-CTA GPC

5.4.1. Conclusions

Synthesis of PS-*b*-PEGMA copolymers was pursued. The first block, PS-CTA, was successfully synthesized at 3 different molecular weights and fully characterized. Chain extension with PEGMA was then pursued but resulted in the formation of homopolymer blends; no block copolymer was observed. It is recommended to lower the MW of the macro-CTA (PS-CTA) to increase the likelihood of successfully forming PS-*b*-PEGMA. If successful, the PS block can be functionalized to PLSS for comparison to analogous RCPs (PEGMA-*r*-PLSS) (Ch.3) and can also be functionalized with more electronegative moieties (e.g., TFSI) to further improve ionic conductivity.

6. Conclusions, recommendations, and future work

The primary objective of this research was to develop a lithium sulfonate-based polymer electrolyte and evaluate its potential for application in lithium metal batteries. PEGMA-*r*-PLSS copolymers were successfully synthesized with a wide range of monomer compositions and fully characterized, including their chemical, thermal, and electrochemical properties. It was confirmed that the optimal [EO]/[Li^+] ratio was around 9:1, as PEGMA-*r*-PLSS-50 showed the best mechanical properties and the second-highest ionic conductivity. Two RCP SIPEs (PEGMA-*r*-PLSS-12 and PEGMA-*r*-PLSS-50) reached high conductivities >10^{-4} S cm^{-1} at 70°C, making them highly relevant for LMB applications.

The copolymers described in this study are highly hygroscopic, which raised concerns about the potential absorption of trace amounts of atmospheric water and its impact on the measured conductivity values. This concern could be mitigated with further tests using a coin cell created in a glovebox. The use of a coin cells was explored within this project, but we experienced short circuiting due to film cracking. Films should be optimized before moving on to coin cell testing; this was not possible at this point due to limited material quantities, but it would be interesting for further study. Additionally, if the material composition and casting process were optimized such that coin cells could be fabricated, lithium transference number and electrochemical stability window are important, relevant properties for LMBs that could be easily tested.

PLVS was successfully synthesized and thoroughly characterized. To observe its effect on conductivity, PEGMA-*r*-PLSS-12 was doped with PVSA at [EO]/[Li^+] ratios of 9:1 and 20:1. No significant enhancement in conductivity was observed. Future work could involve the synthesis of a random PLVS-*r*-PEGMA copolymer or another random copolymer, including PLVS, to further observe the effect on conductivity and confirm the impact of PLVS on ionic conductivity. Also, a copolymer including PLVS, PEGMA, and PLSS could be synthesized to observe the effect on overall properties.

Synthesis of an analog to the RCP was pursued with a PS-*b*-PEGMA copolymer. PS-CTA macro-CTAs were synthesized at three MWs to chain extend with PEGMA. No chain extension was observed despite the lower MW. It is recommended that the MW (>5 kDa) be even lower to improve the chances of forming a BCP. The resulting BCPs can be sulfonated to compare to the

RCPs (Ch.3) for better scalability or functionalized with TFSI-like moieties for enhanced conductivity.

Additional ideas for future work include: 1. Doping PEGMA-*r*-PLSS with other materials to enhance ionic conductivity. 2. Certain inorganic nanoparticles, such as silica (SiO_2), alumina (Al_2O_3), or titanium dioxide (TiO_2), could be added to assist with water retention issues and increase ionic conductivity. 3. Crosslinking to improve mechanical strength by reducing segmental motion, making it a key approach for enhancing durability. 4. Polymer blending to introduce complementary properties that improve both conductivity and mechanical performance.

Overall, this research lays the groundwork for understanding the potential of PEGMA-*r*-PLSS copolymers, with further research likely to improve their properties. These copolymers show promise as candidates for polymer electrolytes in LMBs, potentially solving the issue of dendrite formation and increasing conductivity, leading to improved energy storage technologies.

References

[1] W. Xu, J. Wang, F. Ding, X. Chen, E. Nasybulin, Y. Zhang, J. G. Zhang, Lithium metal anodes for rechargeable batteries. *Energy Environ Sci* **2014**, *7*, 513–537.

[2] Q. Wang, B. Liu, Y. Shen, J. Wu, Z. Zhao, C. Zhong, W. Hu, Confronting the Challenges in Lithium Anodes for Lithium Metal Batteries. *Advanced Science* **2021**, *8*.

[3] J. Gao, C. Wang, D. W. Han, D. M. Shin, Single-ion conducting polymer electrolytes as a key jigsaw piece for next-generation battery applications. *Chem Sci* **2021**, *12*, 13248–13272.

[4] S. K. Sharma, G. Sharma, A. Gaur, A. Arya, F. S. Mirsafi, R. Abolhassani, H. G. Rubahn, J. S. Yu, Y. K. Mishra, Progress in electrode and electrolyte materials: path to all-solid-state Li-ion batteries. *Energy Advances* **2022**, 457–510.

[5] B. Diouf, *Environmental Science: Advances* **2024**, *3*, 332.

[6] H. Zhang, C. Li, M. Piszcz, E. Coya, T. Rojo, L. M. Rodriguez-Martinez, M. Armand, Z. Zhou, Single lithium-ion conducting solid polymer electrolytes: Advances and perspectives. *Chem Soc Rev* **2017**, *46*, 797–815.

[7] S. Li, F. Lorandi, H. Wang, T. Liu, J. F. Whitacre, K. Matyjaszewski, Functional polymers for lithium metal batteries. *Prog Polym Sci* **2021**, *122*.

[8] J. Zhu, Z. Zhang, S. Zhao, A. S. Westover, I. Belharouak, P. F. Cao, Single-Ion Conducting Polymer Electrolytes for Solid-State Lithium–Metal Batteries: Design, Performance, and Challenges. *Adv Energy Mater* **2021**, *11*.

[9] *Future Lithium-ion Batteries*, A. Eftekhari, Ed., The Royal Society of Chemistry, **2019**.

[10] Y. Luo, Z. Rao, X. Yang, C. Wang, X. Sun, X. Li, *Energy Environ Sci* **2024**.

[11] M. K. Aslam, Y. Niu, T. Hussain, H. Tabassum, W. Tang, M. Xu, R. Ahuja, *Nano Energy* **2021**, *86*, 106142.

[12] X. W. Z. L. X. P. Z. L. W. X. Z. Y. X. R. C. Chen, Janus-Pro-7B **2025**.

[13] P. Barai, K. Higa, V. Srinivasan, *Physical Chemistry Chemical Physics* **2017**, *19*, 20493.

[14] T. Ma, X. Ren, L. Hu, W. Teng, X. Wang, G. Wu, J. Liu, D. Nan, X. Yu, Functional Polymer Materials for Advanced Lithium Metal Batteries: A Review and Perspective. *Polymers (Basel)* **2022**, *14*.

[15] A. Murali, R. Ramesh, M. Sakar, S. J. Park, S. S. Han, Unveiling the potential of emergent nanoscale composite polymer electrolytes for safe and efficient all solid-state lithium-ion batteries. *RSC Adv* **2024**, *14*, 30618–30629.

[16] J. Mu, S. Liao, L. Shi, B. Su, F. Xu, Z. Guo, H. Li, F. Wei, Solid-state polymer electrolytes in lithium batteries: latest progress and perspective. *Polym Chem* **2024**, *22*.

[17] A. Méry, S. Rousselot, D. Lepage, M. Dollé, A critical review for an accurate electrochemical stability window measurement of solid polymer and composite electrolytes. *Materials* **2021**, *14*.

[18] H. K. Bergstrom, K. D. Fong, D. M. Halat, C. A. Karouta, H. C. Celik, J. A. Reimer, B. D. McCloskey, *Chem Sci* **2023**, *14*, 6546.

[19] Y. Jiang, X. Yan, Z. Ma, P. Mei, W. Xiao, Q. You, Y. Zhang, Development of the PEO based solid polymer electrolytes for all-solid state lithium ion batteries. *Polymers (Basel)* **2018**, *10*.

[20] K. Aruchamy, S. Ramasundaram, S. Divya, M. Chandran, K. Yun, T. H. Oh, Gel Polymer Electrolytes: Advancing Solid-State Batteries for High-Performance Applications. *Gels* **2023**, *9*.

[21] J. Popovic, D. Brandell, S. Ohno, K. B. Hatzell, J. Zheng, Y. Y. Hu, Polymer-based hybrid battery electrolytes: theoretical insights, recent advances and challenges. *J Mater Chem A Mater* **2021**, *9*, 6050–6069.

[22] E. R. Logan, E. M. Tonita, K. L. Gering, J. Li, X. Ma, L. Y. Beaulieu, J. R. Dahn, *J Electrochem Soc* **2018**, *165*, A21.

[23] R. P. S, V. Prasannavenkadesan, V. Katiyar, A. Ammathnadu Sudhakar, *RSC Applied Polymers* **2025**.

[24] P. Utpalla, S. K. Sharma, S. K. Deshpande, J. Bahadur, D. Sen, M. Sahu, P. K. Pujari, *Physical Chemistry Chemical Physics* **2021**, *23*, 8585.

[25] J. Zhang, J. Zhu, R. Zhao, J. Liu, X. Song, N. Xu, Y. Liu, H. Zhang, X. Wan, Y. Ma, C. Li, Y. Chen, *Energy Environ Sci* **2024**.

[26] J. Li, Y. Cai, H. Wu, Z. Yu, X. Yan, Q. Zhang, T. Gao, K. Liu, X. Jia, Z. Bao, *Adv Energy Mater* **2021**, *11*, 2003239.

[27] B. Boz, H. O. Ford, A. Salvadori, J. L. Schaefer, *Electronic Materials* **2021**, *2*, 154.

[28] K. Deng, T. Guan, F. Liang, X. Zheng, Q. Zeng, Z. Liu, G. Wang, Z. Qiu, Y. Zhang, M. Xiao, Y. Meng, L. Wei, *J Mater Chem A Mater* **2021**, *9*, 7692.

[29] Z. Wang, Z. Li, Y. Jin, W. Liu, L. Jiang, Q. Zhang, *New Journal of Chemistry* **2017**, *41*, 5091.

[30] G. Rollo-Walker, N. Malic, X. Wang, J. Chiefari, M. Forsyth, Development and progression of polymer electrolytes for batteries: Influence of structure and chemistry. *Polymers (Basel)* **2021**, *13*.

[31] X. C. Chen, R. L. Sacci, N. C. Osti, M. Tyagi, Y. Wang, J. K. Keum, N. J. Dudney, *Front Chem* **2021**, *8*.

[32] J. H. H. Wang, C. H. C. Yang, H. Masser, H. S. Shiau, M. V. O'Reilly, K. I. Winey, J. Runt, P. C. Painter, R. H. Colby, *Macromolecules* **2015**, *48*, 7273.

[33] S. Feng, D. Shi, F. Liu, L. Zheng, J. Nie, W. Feng, X. Huang, M. Armand, Z. Zhou, *Electrochim Acta* **2013**, *93*, 254.

[34] D. Devaux, L. Liénafa, E. Beaudoin, S. Maria, T. N. T. Phan, D. Gigmes, E. Giroud, P. Davidson, R. Bouchet, *Electrochim Acta* **2018**, *269*, 250.

[35] Q. Ma, H. Zhang, C. Zhou, L. Zheng, P. Cheng, J. Nie, W. Feng, Y. Hu, H. Li, X. Huang, L. Chen, M. Armand, Z. Zhou, *Angewandte Chemie* **2016**, *128*, 2567.

[36] N. Meng, Y. Ye, Z. Yang, H. Li, F. Lian, Developing Single-Ion Conductive Polymer Electrolytes for High-Energy-Density Solid State Batteries. *Adv Funct Mater* **2023**, *33*.

[37] C. H. Park, Y. K. Sun, D. W. Kim, "Blended polymer electrolytes based on poly(lithium 4-styrene sulfonate) for the rechargeable lithium polymer batteries," Electrochimica Acta, 30 November **2004**.

[38] Z. Xue, D. He, X. Xie, *J Mater Chem A Mater* **2015**, *3*, 19218.

[39] C. W. H. Rajawasam, O. J. Dodo, M. A. S. N. Weerasinghe, I. O. Raji, S. V. Wanasinghe, D. Konkolewicz, N. De Alwis Watuthanthrige, Educational series: characterizing crosslinked polymer networks. *Polym Chem* **2023**, *15*, 219–247.

[40] J.-D. Jeon, M.-J. Kim, S.-Y. Kwak, *J Power Sources* **2006**, *162*, 1304.

[41] J. Hu, W. Wang, R. Yu, M. Guo, C. He, X. Xie, H. Peng, Z. Xue, *RSC Adv* **2017**, *7*, 54986.

[42] V. P. H. Huy, S. So, J. Hur, Inorganic fillers in composite gel polymer electrolytes for high-performance lithium and non-lithium polymer batteries. *Nanomaterials* **2021**, *11*, 1–40.

[43] H. Feng, X. Lu, W. Wang, N. G. Kang, J. W. Mays, *Polymers (Basel)* **2017**, *9*.

[44] W. S. Young, W. F. Kuan, T. H. Epps, Block copolymer electrolytes for rechargeable lithium batteries. *J Polym Sci B Polym Phys* **2014**, *52*, 1–16.

[45] N. Hendeniya, K. Hillery, B. S. Chang, Processive Pathways to Metastability in Block Copolymer Thin Films. *Polymers (Basel)* **2023**, *15*.

[46] D. J. Keddie, *Chem Soc Rev* **2014**, *43*, 496.

[47] V. Vijayakumar, B. Anothumakkool, S. Kurungot, M. Winter, J. R. Nair, *Energy Environ Sci* **2021**, *14*, 2708.

[48] Z. Li, H. Yong, K. Wang, Y. N. Zhou, J. Lyu, L. Liang, D. Zhou, *Chemical Communications* **2023**, *59*, 4142.

[49] N. P. Truong, G. R. Jones, K. G. E. Bradford, D. Konkolewicz, A. Anastasaki, *Nat Rev Chem* **2021**, *5*, 859.

[50] P. Zhou, X. Zhang, Y. Xiang, K. Liu, Strategies to enhance Li+ transference number in liquid electrolytes for better lithium batteries. *Nano Res* **2023**, *16*, 8055–8071.

[51] Z. Guo, J. Zhu, J. Feng, S. Du, *RSC Adv* **2015**, *5*, 69514.

[52] P. Liu, M. J. Counihan, Y. Zhu, J. G. Connell, D. Sharon, S. N. Patel, P. C. Redfern, P. Zapol, N. M. Markovic, P. F. Nealey, L. A. Curtiss, S. Tepavcevic, *Advanced Energy and Sustainability Research* **2022**, *3*.

[53] N. S. Kwon, S. W. Ryu, *Solid State Ion* **2021**, *361*.

[54] I. Ando, "Some aspects of the NMR chemical shift/structure correlation in the structural characterization of polymers and biopolymers," Polymer Journal, August **2012**.

[55] P. Balding, R. Borrelli, R. Volkovinsky, P. S. Russo, *Macromolecules* **2022**, *55*, 1747.

[56] L. Porcarelli, A. S. Shaplov, M. Salsamendi, J. R. Nair, Y. S. Vygodskii, D. Mecerreyes, C. Gerbaldi, *ACS Appl Mater Interfaces* **2016**, *8*, 10350.

[57] P. Raut, S. Li, Y. M. Chen, Y. Zhu, S. C. Jana, *ACS Omega* **2019**, *4*, 18203.

[58] W. R. Fullerton, C. Y. Li, *ACS Appl Polym Mater* **2024**, *6*, 7468.

[59] L. A. M. Mahmoud, J. L. Rowlandson, D. J. Fermin, V. P. Ting, S. Nayak, *RSC Applied Interfaces* **2025**.

[60] N. G. Ningappa, A. K. Madikere Raghunatha Reddy, K. Zaghib, Advanced Polymer Electrolytes in Solid-State Batteries. *Batteries* **2024**, *10*.

[61] J. Chattopadhyay, T. S. Pathak, D. M. F. Santos, Applications of Polymer Electrolytes in Lithium-Ion Batteries: A Review. *Polymers (Basel)* **2023**, *15*.

[62] N. M. Nurazzi, M. R. M. Asyraf, M. Rayung, M. N. F. Norrrahim, S. S. Shazleen, M. S. A. Rani, A. R. Shafi, H. A. Aisyah, M. H. M. Radzi, F. A. Sabaruddin, R. A. Ilyas, E. S. Zainudin, K. Abdan, Thermogravimetric analysis properties of cellulosic natural fiber polymer composites: A review on influence of chemical treatments. *Polymers (Basel)* **2021**, *13*.

[63] S. N. F. Yusuf, S. Z. Yusof, M. Z. Kufian, L. P. Teo, Preparation and electrical characterization of polymer electrolytes: A review, **2019**, www.sciencedirect.comwww.materialstoday.com/proceedings.

[64] T. Rasheed, A. Naveed, J. Chen, B. Raza, J. Wang, *Energy Storage Mater* **2022**, *45*, 1012.

[65] M. Petrowsky, R. Frech, *Journal of Physical Chemistry B* **2009**, *113*, 5996.

[66] NEI CORPORATION, **2017**.

[67] J. Chattopadhyay, T. S. Pathak, D. M. F. Santos, Applications of Polymer Electrolytes in Lithium-Ion Batteries: A Review. *Polymers (Basel)* **2023**, *15*.

[68] K. Noori, B. A. Olsen, A. Rodin, *Phys Rev Res* **2024**, *6*.

[69] S. Choudhury, S. Stalin, D. Vu, A. Warren, Y. Deng, P. Biswal, L. A. Archer, *Nat Commun* **2019**, *10*.

[70] Z. Li, J. Fu, X. Zhou, S. Gui, L. Wei, H. Yang, H. Li, X. Guo, Ionic Conduction in Polymer-Based Solid Electrolytes. *Advanced Science* **2023**, *10*.

[71] T. L. Chen, R. Sun, C. Willis, B. Krutzer, B. F. Morgan, F. L. Beyer, K. S. Han, V. Murugesan, Y. A. Elabd, *Polymer (Guildf)* **2020**, *209*.

[72] H. Ohno, N. Kobayashi, S. Takeoka, H. Ishizaka, E. Tsuchida, *Solid State Ion* **1990**, *40–41*, 655.

[73] X. Yu, Z. Jiang, R. Yuan, H. Song, A Review of the Relationship between Gel Polymer Electrolytes and Solid Electrolyte Interfaces in Lithium Metal Batteries. *Nanomaterials* **2023**, *13*.

[74] T. Hussain, M. Ansari, N. M. Ranjha, I. U. Khan, Y. Shahzad, *The Scientific World Journal* **2013**, *2013*.

[75] S. J. Park, S. G. Yoon, H. Il Kim, K. M. Shin, S. I. Kim, S. J. Kim, "Polyacrylic acid/poly(vinyl sulfonic acid, sodium salt) copolymer hydrogel actuator under an electric field," Smart Structures and Materials 2004: Electroactive Polymer Actuators and Devices (EAPAD), SPIE, 27 July **2004**.

[76] T. Okayasu, T. Hibino, H. Nishide, *Macromol Chem Phys* **2011**, *212*, 1072.

[77] B. L. Rivas, L. N. Schiappacasse, *J Appl Polym Sci* **2003**, *88*, 1698.

[78] A. Y. Gyurova, S. Halacheva, E. Mileva, *RSC Adv* **2017**, *7*, 13372.

[79] N. Yazie, D. Worku, N. Gabbiye, A. Alemayehu, Z. Getahun, M. Dagnew, Development of polymer blend electrolytes for battery systems: recent progress, challenges, and future outlook. *Mater Renew Sustain Energy* **2023**, *12*, 73–94.

[80] G. Xi, M. Xiao, S. Wang, D. Han, Y. Li, Y. Meng, Polymer-Based Solid Electrolytes: Material Selection, Design, and Application. *Adv Funct Mater* **2021**, *31*.

[81] L. A. Utracki, Compatibilization of polymer blends. *Canadian Journal of Chemical Engineering* **2002**, *80*, 1008–1016.

[82] B. E. CONWAY, E. AYRANCI, *J Solution Chem* **1999**, *28*, 163.

[83] J. Shi, H.-D. Nguyen, Z. Chen, R. Wang, D. Steinle, L. Barnsley, J. Li, H. Frielinghaus, D. Bresser, C. Iojoiu, E. Paillard, *Energy Materials* **2023**, *3*.

[84] K. M. Meek, Y. A. Elabd, *Macromol Rapid Commun* **2016**, *37*, 1200.

Appendix A. Additional Characterization Figures

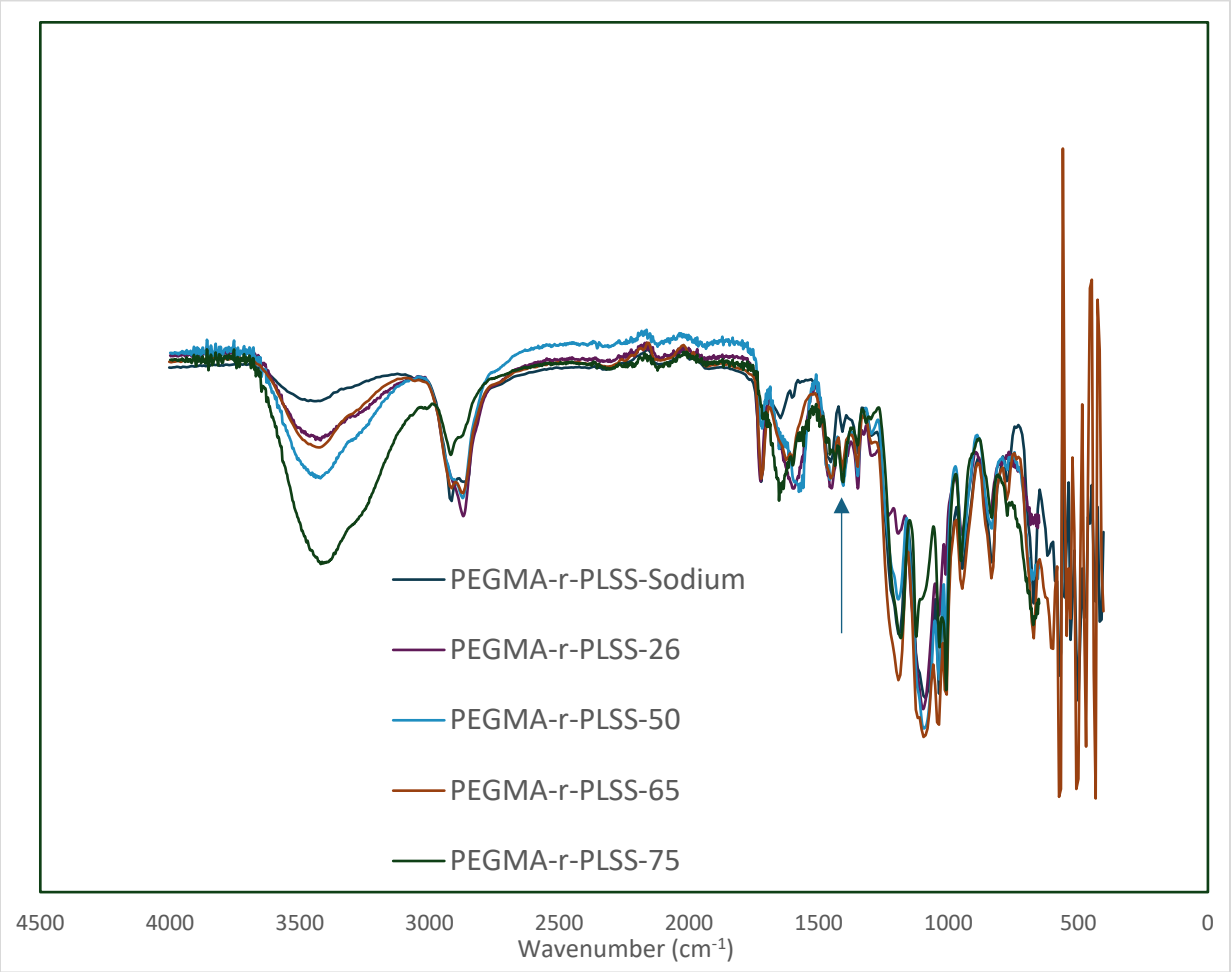

A.1 FTIR of PEGMA-r-PLSS samples indicating Li+ peak

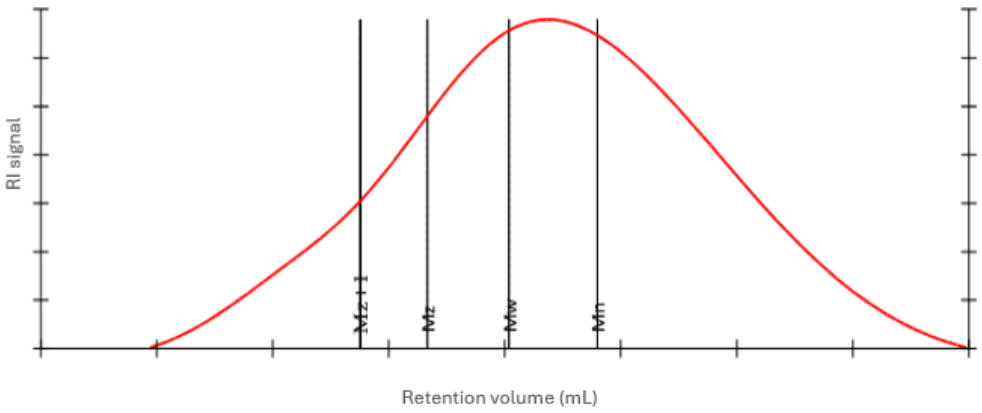

A.2 GPC trace of PEGMA-r-PLSS-12

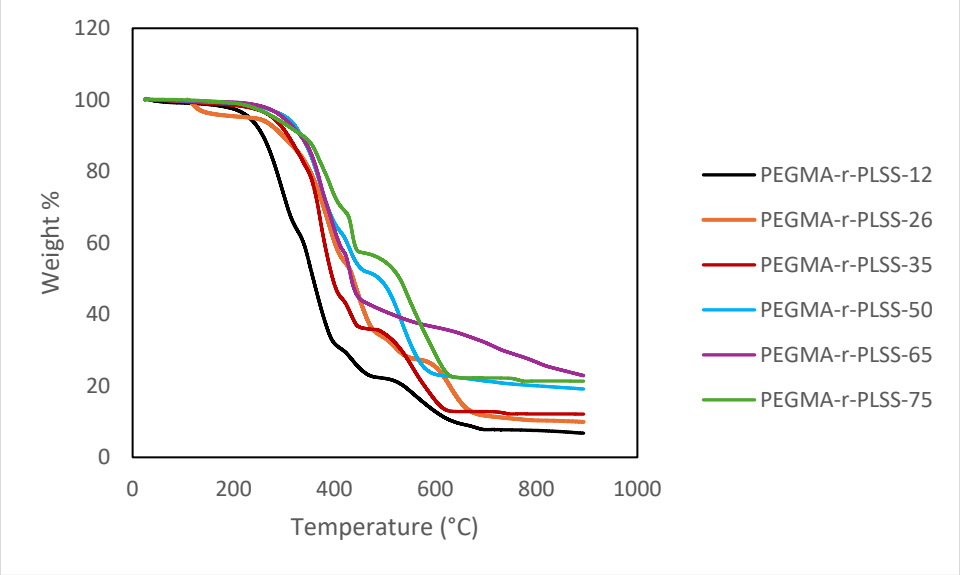

A.3 TGA curves of all PEGMA-r-PLSS samples

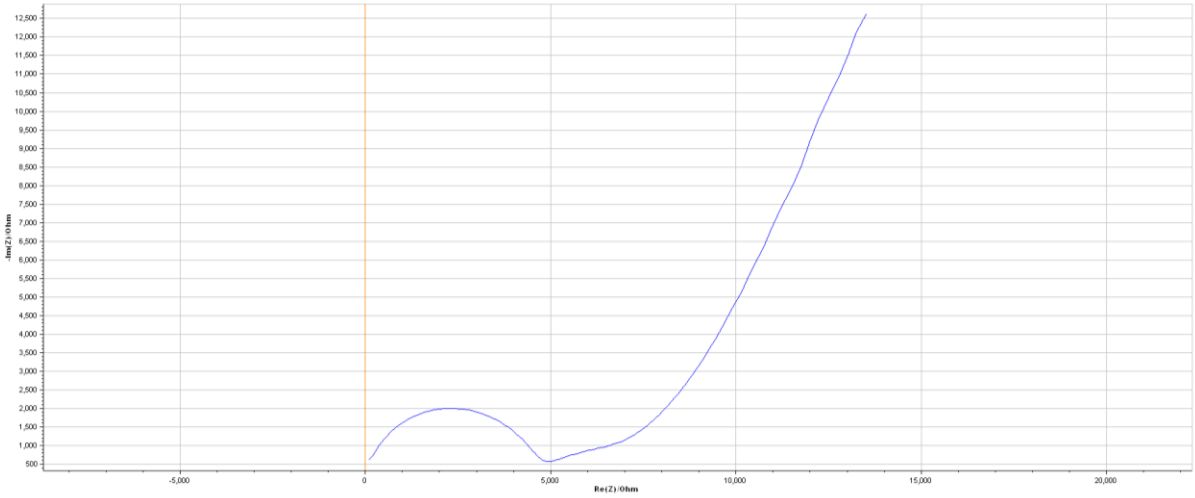

A.4 Example Nyquist plot of EIS data

Appendix B: Health and safety

Laboratory considerations

When performing polymer synthesis and characterization for single-ion polymer electrolytes, laboratory safety considerations are crucial to prevent exposure to hazardous chemicals and ensure a safe working environment. Key considerations include:

Personal Protective Equipment (PPE):

- **Gloves**: Wear chemically resistant gloves (e.g., nitrile or neoprene) to prevent skin contact with chemicals.
- **Safety goggles or face shield**: Protect your eyes from chemical splashes.
- **Lab coat**: A flame-retardant lab coat should be worn to protect against chemical spills.
- **Respiratory protection**: A respirator may be required depending on the chemicals used (e.g., solvents or acids). Check if required using Material Safety Data Sheets (MSDS) or Safety Data Sheets (SDS).

Chemical Hazards:

- **Monomers**: Monomers, especially in single-ion polymer electrolytes, can pose various health and safety risks. Depending on the type of monomer, different chemical hazards should be considered. Check Material Safety Data Sheets (MSDS) or Safety Data Sheets (SDS) to confirm potential hazards.
- **Solvents**: Many solvents used in polymer synthesis (e.g., DMF) are flammable and may also be toxic or irritants. Check Material Safety Data Sheets (MSDS) or Safety Data Sheets (SDS) to confirm potential hazards.
- **Toxicity**: Some chemicals can be harmful if inhaled, ingested, or absorbed through the skin. Toxicity warnings should be checked by reading Material Safety Data Sheets (MSDS) or Safety Data Sheets (SDS).

Proper Ventilation:

- **Fume hood**: Perform polymer synthesis reactions in a well-ventilated fume hood to minimize exposure to harmful vapors and fumes from monomers, solvents, and reagents.

- **Ventilation system**: Ensure the laboratory has a ventilation system to control chemical vapors and ensure worker safety.

Waste Disposal:

- **Chemical waste**: Safely dispose of solvents, acids, and other waste by following institutional and environmental regulations.
- **Sharps disposal**: Using needles, syringes, or other sharp instruments, use proper sharps disposal containers.

Emergency Procedures:

- **Eyewash stations and safety showers**: Ensure functioning eyewash stations and safety showers are nearby in case of chemical exposure.
- **First aid**: Familiarize yourself with first-aid procedures for chemical burns or inhalation and have the Material Safety Data Sheets (MSDS) or Safety Data Sheets (SDS) of all chemicals on hand.

Table B1. Chemical Hazards and personal protective equipment (PPE) required

Chemical	Potential Hazards	Required PPE
D_2O (Deuterium oxide)	Low toxicity, avoid ingestion, inhalation, and skin contact	Lab coat, gloves, safety goggles, fume hood
PEGMA (Poly(ethylene glycol) methyl ether methacrylate)	Irritant to eyes and skin, harmful if ingested	Lab coat, gloves, safety goggles, fume hood
VSA (Vinyl sulfonic acid sodium salt)	Corrosive to skin and eyes, toxic by ingestion or inhalation	Lab coat, gloves (neoprene or nitrile), safety goggles, fume hood
AIBN (2,2′-Azobis-(isobutyronitrile))	Hazardous when heated, toxic, irritant, and a fire hazard	Lab coat, gloves, safety goggles, flame arrestor, fume hood
APS (Ammonium persulfate)	Oxidizing agent, irritant to skin and eyes, toxic if ingested	Lab coat, gloves, safety goggles, fume hood
LiOH (Lithium hydroxide monohydrate)	Corrosive to eyes, skin, and respiratory system	Lab coat, gloves (neoprene or nitrile), safety goggles, fume hood
DMF (N,N-Dimethylformamide)	Harmful if inhaled, absorbed through skin, or ingested, irritant to eyes and skin	Lab coat, gloves, safety goggles, fume hood, respirator if needed
DMSO (Dimethylsulfoxide)	Skin absorption, potential for carrying other toxic substances into the body	Lab coat, gloves, safety goggles, fume hood
$CDCl_3$ (Deuterated chloroform)	Harmful if inhaled, ingested, or absorbed through skin, irritant to eyes	Lab coat, gloves, safety goggles, fume hood
Styrene	Flammable, toxic by inhalation, irritant to eyes and skin, possible carcinogen	Lab coat, gloves (nitrile), safety goggles, flame arrestor, fume hood
Sulfonated Styrene	Irritant, toxic, potentially flammable	Lab coat, gloves, safety goggles, fume hood